

Multimodal Image Synthesis and Editing: A Survey

Fangneng Zhan, Yingchen Yu, Rongliang Wu, Jiahui Zhang, Shijian Lu[§], Lingjie Liu
 Adam Kortylewski, Christian Theobalt, Eric Xing, *Fellow, IEEE*

Abstract—As information exists in various modalities in real world, effective interaction and fusion among multimodal information plays a key role for the creation and perception of multimodal data in computer vision and deep learning research. With superb power in modeling the interaction among multimodal information, multimodal image synthesis and editing has become a hot research topic in recent years. Instead of providing explicit guidance for network training, multimodal guidance offers intuitive and flexible means for image synthesis and editing. On the other hand, this field is also facing several challenges in alignment of multimodal features, synthesis of high-resolution images, faithful evaluation metrics, etc. In this survey, we comprehensively contextualize the advance of the recent multimodal image synthesis and editing and formulate taxonomies according to data modalities and model types. We start with an introduction to different guidance modalities in image synthesis and editing, and then describe multimodal image synthesis and editing approaches extensively according to their model types. After that, we describe benchmark datasets and evaluation metrics as well as corresponding experimental results. Finally, we provide insights about the current research challenges and possible directions for future research. A project associated with this survey is available at <https://github.com/fnzhan/MISE>.

Index Terms—Multimodality, Image Synthesis & Editing, GANs, Auto-regressive Models, Diffusion Models, Neural Fields.

1 INTRODUCTION

HUMANS are naturally capable of imaging a scene according to a piece of visual, text or audio description. However, the underlying processes are not that straightforward to deep neural networks due to the inherent modality gap. This *modality gap* for visual perception can be boiled down to *intra-modal gap* between visual clues and real images and *cross-modal gap* between non-visual clues and real images. Targeting to mimic human imagination and creativity in the real world, the tasks of Multimodal Image Synthesis and Editing (MISE) provide profound insights about how deep neural networks correlate multimodal information with image attributes.

Image synthesis and editing aims to create realistic images or edit real images with natural textures. In the last few years, it has witnessed very impressive progress thanks to the advance of deep learning especially Generative Adversarial Networks (GANs) [1]. To achieve more controllable generation, a popular line of research focuses on generating and editing images conditioned on certain guidance. Typically, visual clues, such as segmentation maps and sketch maps, have been widely adopted for image synthesis and editing [2]–[4]. Beyond the intra-modal guidance of visual clues, cross-modal guidance such as texts, audios, and scene graph provides an alternative but often more intuitive and flexible way of expressing visual concepts. However,

effective retrieval and fusion of heterogeneous information from data of different modalities remains a big challenge in multimodal image synthesis and editing.

As a pioneering effort in multimodal image synthesis, [10] shows that recurrent variational auto-encoder could generate novel visual scenes conditioned on image captions. The research of multimodal image synthesis is then greatly advanced with the prosperity of Generative Adversarial Networks (GANs) [1]–[3], [11]–[16]. Originating from the Conditional GANs (CGANs) [11], various multimodal signals have been investigated for conditional generation. Typically, multimodal signals are firstly encoded into features to align with the feature spaces of GANs. Then, the encoded features can serve as input to conditional GANs or be incorporated into the generation process. To achieve consistency between conditions and generated images, the encoded features are usually concatenated with image features to serve as input of discriminator. With the prosperity of large scale GANs, a bunch of models [17]–[20] have been developed to synthesize images with high quality and diversity from random noise input. As recent studies show that rich semantic information is encoded in the latent space of GANs [21], GAN inversion [22], [23] is introduced to invert a given image back into the latent space of a pretrained GAN, yielding an inverted code that can faithfully reconstruct the given image via the generator. Since GAN inversion allows to control attribute directions in latent spaces, pre-trained GANs become applicable to MISE by manipulating the latent code ([24], [25]), without requiring ad-hoc supervision or cumbersome model training.

Currently, a CNN architecture is still widely adopted in GANs, which hinders GANs from handling multimodal data in a unified manner. With the prevalence of Transformer model [26] which naturally allows cross-modal in-

• F. Zhan is with the Max Planck Institute for Informatics, Germany and the S-Lab, Nanyang Technological University, Singapore.
 • Y. Yu, R. Wu, J. Zhang and S. Lu are with the Nanyang Technological University, Singapore.
 • L. Liu, A. Kortylewski and C. Theobalt are with the Max Planck Institute for Informatics, Germany.
 • E. Xing is with the Carnegie Mellon University, USA and the Mohamed bin Zayed University of Artificial Intelligence, UAE.
 • [§] denotes corresponding author, E-mail: shijian.lu@ntu.edu.sg.

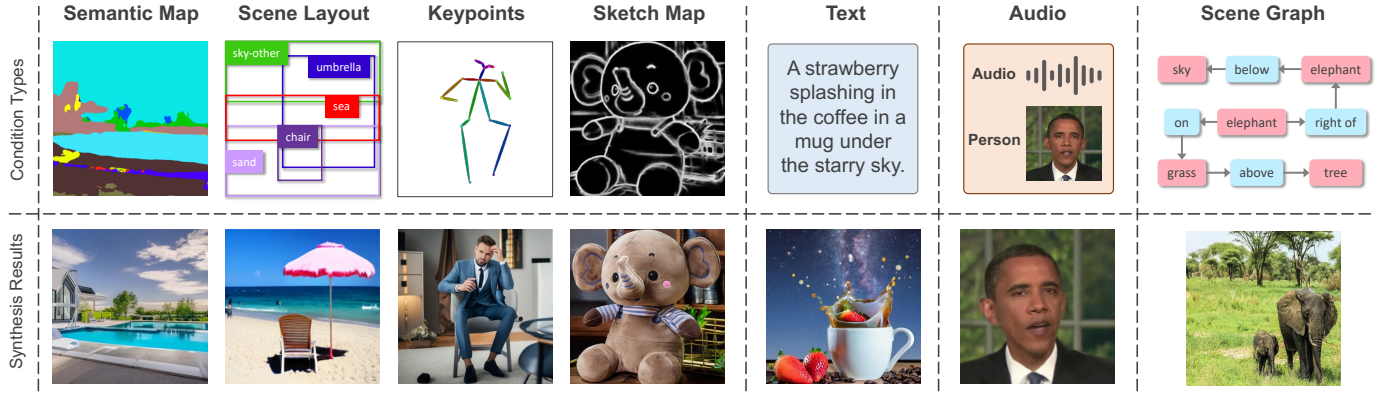


Fig. 1. Typical multimodal guidance in image synthesis and editing: The first row shows intra-modal (i.e., visual) guidance including semantic maps, scene layouts, keypoints, sketch maps, and cross-modal guidance including text, audio and scene graph. The samples are from [5]–[9].

put, impressive improvements have been achieved in different modality, such as language models [27], image generative pre-training [28], and audio generation [29]. These recent advances fueled by Transformer suggest a possible route for auto-regressive models [30] in multimodal image synthesis and editing by accommodating the long-range dependency of sequences. Notably, both multimodal guidance and images can be represented in a common form of discrete tokens. For instance, texts can be naturally denoted by token sequence; audio and visual guidance including images can be represented as token sequences via VQ-VAE [31]. With such unified discrete representation, the correlation between multimodal guidance and images can be accommodated via auto-regressive models. Following this line of research, plenty of effort has been devoted to push the boundary of MISE, e.g., employing a large-scale auto-regressive Transformer with numerous text-image pairs to produce a high-fidelity text-to-image generation [32], combining VQ-VAE with perceptual loss [33] to learn rich image representation [33], introducing 3D Transformer encoder-decoder framework to achieve unified generation or editing of images and videos [34], etc.

Recently, diffusion models have emerged as a popular line of likelihood-based generative models which possess several desirable properties like stationary training objective and good scalability. As diffusion models have demonstrated superior image synthesis capability compared with SOTA GANs [35], diffusion-based MISE starts to garner great attention from the research community. Similar to GANs, the framework of diffusion-based MISE can boil down to two paradigms, e.g., training conditional diffusion models and relying on pre-trained diffusion models. Developing conditional diffusion models is relatively straightforward, by incorporating the provided condition into the denoising diffusion process. This paradigm is widely adopted in SOTA methods to yield unprecedented yet faithful generation [36]–[38]. However, training diffusion models from scratch involves high computational cost, thus another line of research leverages pre-trained diffusion models to achieve MISE. Typically, with pre-trained unconditional models, a guidance function [35], [39] can be introduced to achieve conditional generation by measuring the consistency between the generated and guidance in the reverse

sampling process. Besides, MISE also can be achieved by adapting pre-trained diffusion models [40] or manipulating latent embeddings [41]–[43] in a similar manner to GAN inversion.

Most aforementioned methods work for 2D images regardless the 3D essence of real world. With the recent advance of neural fields, especially Neural Radiance Fields (NeRF) [44], 3D-aware image synthesis and editing have attracted increasing attention from the community. Distinct from synthesis and editing on 2D images, 3D-aware MISE poses a bigger challenge thanks to the lack of data and requirement of multi-view consistency during synthesis or editing. For per-scene optimization NeRF, pre-trained models (e.g., CLIP [45] and Stable Diffusion [46]) are usually employed to drive the NeRF optimization for view synthesis and editing, by connecting NeRF-rendered images and the multimodal guidance (e.g., texts). Under generative setting, the MISE can be performed via conditional NeRF or NeRF inversion. For conditional NeRF, the multimodal guidance is usually encoded to a 1-D feature vector, which is further incorporated into the radiance field for conditional NeRF training. For NeRF inversion, the multimodal guidance is usually embedded into the latent space of a pre-trained generative NeRF, where various 3D-aware synthesis or editing can be performed naturally.

The contributions of this survey can be summarized in the following aspects:

- This survey covers extensive literature with regard to multimodal image synthesis and editing, and catalogues existing methods in a rational and structured framework.
- We provide a foundation of different types of guidance modality underlying multimodal image synthesis and editing tasks and elaborate the specifics of encoding approaches associated with the guidance modalities.
- We develop a taxonomy of the recent approaches according to the essential models and highlight the major strengths and weaknesses of existing models.
- This survey provides an overview of various datasets and evaluation metrics in multimodal image synthesis and editing, and critically evaluates the performance of contemporary methods.
- We summarize the open challenges in the current research and share our humble opinions on promising areas and

directions for future research.

The remainder of this survey is organized as follows. Section 2 presents the foundation of popular guidance modalities in multimodal image synthesis and editing. Section 3 provides a comprehensive overview and description of MISE methods with detailed pipelines. Section 4 reviews the common datasets and evaluation metrics, with quantitative experimental results of typical methods. In Section 5, we discuss the main challenges and future research directions for multimodal image synthesis and editing. Some social impact analysis and concluding remarks are drawn in Section 6 and Section 7, respectively.

2 MODALITY FOUNDATIONS

Each source or form of information can be called a modality. For example, people have the sense of touch, hearing, sight, and smell; the medium of information includes voice, video, text, etc.; data are recorded by various sensors such as radar, infrared, and accelerometer. In terms of image synthesis and editing, we group the modality guidance as visual guidance, text guidance, audio guidance, and other modality guidance. Detailed description of each modality guidance together with related processing methods will be presented in the following subsections.

2.1 Visual Guidance

Visual guidance has attracted broad attention in image synthesis and editing as realistic images can be naturally induced from visual guidance. Typically, visual guidance represents certain image properties in pixel space such as segmentation maps [2], [3], keypoints [47]–[49], sketch maps (including edge maps and line maps which are special cases of sketch) [50]–[58], and scene layouts [59]–[63] as illustrated in Fig. 1. Besides, several studies investigate image synthesis conditioned on depth map [33], mouse trace [64], illumination map [65]–[67], etc. The visual guidance can be obtained by employing pre-trained models (e.g., segmentation model, depth predictor, pose predictor), applying algorithms (e.g., Canny edges, Hough lines), or relying on manual effort (e.g., manual annotation, human scribbles). By editing the visual guidance, such as semantic maps, image synthesis methods can be directly adapted for image manipulation tasks [68], [69].

Visual Encoding. As represented in 2D pixel space, these visual clues can be regarded as certain type of images which can be directly encoded following various image encoding approaches (e.g., CNN and Transformer).

2.2 Text Guidance

Compared to visual guidance, such as segmentation maps and sketch maps, text prompt provides a more flexible way to express visual concepts. The text-to-image synthesis task [70]–[74] aims to produce clear, photo-realistic images with high semantic relevance to the corresponding text guidance. This task is very challenging as text descriptions are often ambiguous and can lead to numerous images with correct semantics. In addition, images and texts come with heterogeneous features, which makes it hard to learn

accurate and reliable mapping across the two modalities. Thus, learning an accurate embedding of text description plays an important role in text-guided image synthesis and editing.

Text Encoding. Learning useful encodings from textual representations is a non-trivial task. There are a number of traditional text representations, such as Word2Vec [75] and Bag-of-Words [76]. With the prevalence of deep neural networks, Recurrent Neural Network (RNN) [72] and LSTM [77] are widely adopted to encode texts as features [78]. With the development of pre-trained models in natural language processing field, several studies [79], [80] also explore to perform text encoding by leveraging large-scale pre-trained language models such as BERT [81]. Besides, Contrastive Language-Image Pre-training (CLIP) [45] yields informative text embeddings by learning the alignment of images and the corresponding captions from a large amount of image-text pairs, and has been widely adopted for text encoding.

2.3 Audio Guidance

Hearing helps humans to sense the world. The relation between auditory contents and visual contents has been explored in previous cross-modal learning and generation research [82]–[84], demonstrating that specific visual contents can be attended while the corresponding audio is pronounced. Sounds can not only interact with visual contents but also capture rich semantic information. As proved in SoundNet [85], a deep model can learn to identify scenes and objects by using auditory contents only.

Audio Encoding. An audio sequence can be generated from given videos where deep convolution network is employed to extract features from video screenshots followed by LSTM [86] to generate audio waveform of the corresponding input video [87]. An input audio segment can also be represented by a sequence of features which can be spectrograms, fBanks, Mel-Frequency Cepstral Coefficients (MFCCs), and the hidden layer outputs of the pre-trained SoundNet model [85]. In talking face generation [88], Action Units (AUs) [89] has also been widely adopted to convert the driving audio into coherent visual signals for talking face generation.

2.4 Other Modality Guidance

Several other types of guidance have also been investigated to guide multimodal image synthesis and editing.

Scene Graph. Scene Graphs represent scenes as directed graphs, where nodes are objects and edges give relationships between objects. Image generation conditioned on scene graphs allows to reason explicit object relationships and synthesize faithful images with complex scene relationships. The guided scene graph can be encoded through a graph convolution network [90] which predicts object bounding boxes to yield a scene layout. For example, to derive each individual subject-predicate-object relation, Vo *et al.* [91] propose to predict relation units between objects, which is converted to a visual layout via convolutional LSTM [92].

Brain Signal. Treating brain signals as a modality to synthesize or reconstruct visual images offers an exciting way to understand brain activity and facilitate brain-computer

interfaces. Recently, several studies explore to generate images from functional magnetic resonance imaging (fMRI). For example, Fang *et al.* [93] decode shape and semantic representations from the lower and higher visual cortex respectively, and then fuse them to generate images via GAN. Lin *et al.* [94] propose to map fMRI signals into the latent space of pretrained StyleGAN to enable conditional generation and leverage CLIP to incorporate text descriptions of images to facilitate the mapping. On top of it, Takagi and Nishimoto [95] leverage pretrained latent diffusion models (LDM) [46] to generate high-resolution images and quantitatively interpret each component in LDM by mapping them into distinct brain regions.

3 METHODS

We broadly categorize the methods for multimodal image synthesis and editing (MISE) into five categories: the GAN-based methods (Sec. 3.1), the Autoregressive methods (Sec. 3.2), the Diffusion-based methods (Sec. 3.3), the Neural Field methods (Sec. 3.4), and other methods (Sec. 3.5). We first discuss the GAN-based methods, which generally rely on GANs and their inversion. We then discuss the prevailing Autoregressive and Diffusion-based frameworks comprehensively. After that, we introduce neural fields for the challenging task of 3D-aware MISE. Later, we present several other methods for visual synthesis and editing under the context of multimodal guidance. Finally, we compare and discuss the strengths and weaknesses of different generation architectures.

3.1 GAN-based Methods

GAN-based methods have been widely adopted for various MISE tasks by either developing conditional GANs (Sec. 3.1.1) or leveraging pre-trained unconditional GANs (Sec. 3.1.2). For conditional GANs, multimodal condition can be directly incorporated into the generator to guide the generation process. For pre-trained unconditional GANs, GAN inversion is usually employed to perform various MISE tasks by operating latent codes in latent spaces.

3.1.1 Conditional GANs

Conditional Generative Adversarial Networks (CGANs) [11] are extensions of the popular GAN architecture which allow for image generation with specific characteristics or attributes. The key idea behind CGANs is to condition the generation process on additional information, such as multimodal guidance in MISE tasks. This is achieved by feeding the additional information into both the generator and discriminator networks as extra guidance. The generator then learns to generate samples that not only fool the discriminator but also match the specified conditional information. In recent years, a range of designs have significantly boosted the performance of CGANs for MISE [73].

Condition Incorporation. To steer the generation process, it is necessary to incorporate multimodal conditions into the network effectively as shown in Fig. 2. Generally, multimodal guidance can be uniformly encoded as 1-D features which can be concatenated with the feature

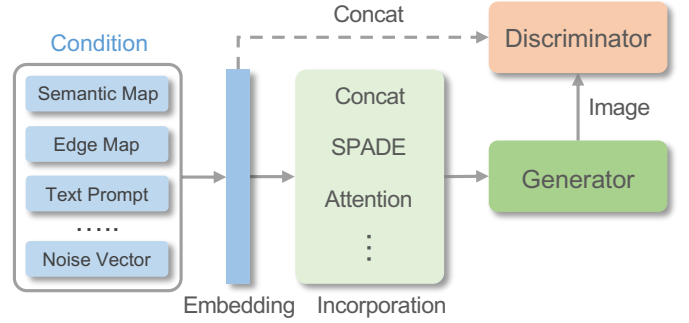


Fig. 2. Illustration of conditional GAN framework with different condition incorporation mechanisms.

in networks [11], [72], [96]. For visual guidance that is spatially aligned with the target image, the condition can be directly encoded as 2D features which provide accurate spatial guidance for generation or editing [2]. However, the encoded 2D features struggle to capture complex scene structural relationships between the guidance and real images when there exists very different views or severe deformations. Under such circumstances, an attention module can be employed to align the guidance with the target image as in [7], [97]–[99]. Moreover, naively encoding the visual guidance with deep networks is suboptimal as part of the guidance information tends to be lost in normalization layers. Thus, a spatially-adaptive de-normalization (SPADE) [3] is introduced to inject the guided feature effectively, which is further extended to a semantic region-adaptive normalization [100] to achieve region-wise condition incorporation. Besides, by assessing the similarity between generated images and conditions, an attentional incorporation mechanism [77], [101]–[104] can be employed to direct the generator’s attention to particular image regions during generation, which is particularly advantageous when dealing with complex conditional information, such as texts. Notably, complex conditions also can be mapped to an intermediary representation which facilitates more faithful image generation, *e.g.*, audio clip can be mapped to facial landmarks [105], [106] or 3DMM parameters [107] for talking-face generation. For sequential conditions such as audios [16], [88], [96], [105], [108]–[111], a recurrent condition incorporation mechanism is also widely adopted to account for temporal dependency such that smooth transition can be achieved in sequential conditions.

Model Structure. Conditional generation of high-resolution images with fine details is challenging and computationally expensive for GANs. Coarse-to-fine structures [58], [70], [71], [74], [118], [119] help address these issues by gradually refining the generated images or features from low resolutions to high resolutions. By generating coarse images or features first and then refining them as shown in Fig. 3 (a), the generator network can focus on capturing the overall structure of the image before moving on to the fine details, which leads to more efficient training and higher generation quality. Not only generator, many discriminator networks [112], [118] also operate at multiple levels of resolution to efficiently differentiate high-resolution images and avoid potentially overfitting. On

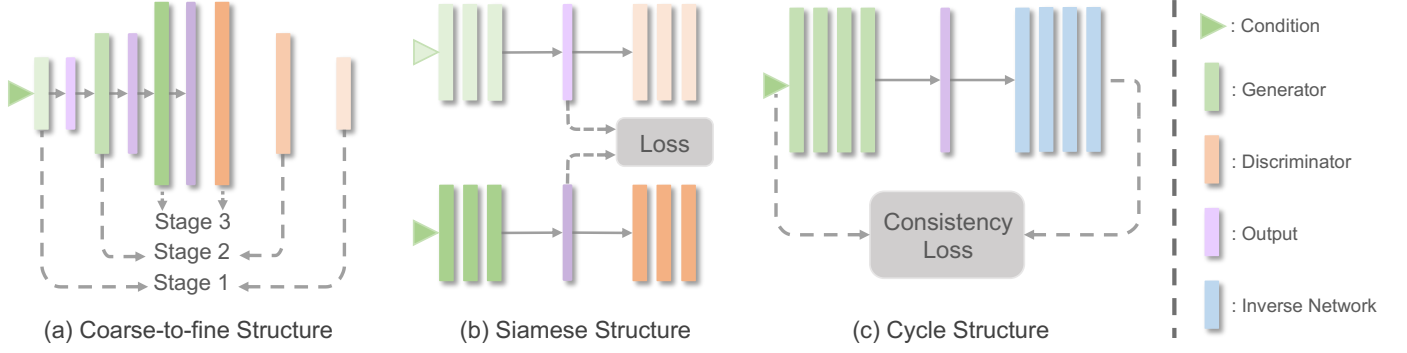


Fig. 3. Illustration of different model structures in conditional GANs, including (a) coarse-to-fine structure [70], [71], [112], (b) siamese structure [102], [113], [114] and (c) cycle structure [78], [115]–[117].

the other hand, as a scene can be depicted with diverse linguistic expressions, generating images with consistent semantics regardless of the expression variants presents a significant challenge. Multiple pieces of research employ a siamese structure with two generation branches to facilitate the semantic alignment as shown in Fig. 3 (b). With a pair of conditions for the two branches, a contrastive loss can be adopted to minimize the distance between positive pairs (two text prompts describe the same scene) and maximize the distance between negative pairs (two prompts describe different scenes) [102], [113], [114]. Besides, an intra-domain transformation loss [120] can also be employed in siamese structure to preserve key characteristics during generation. Except for above structures, a cycle structure also has been explored in series of conditional GANs to preserve key information in generation process, as shown in Fig. 3 (c). Specifically, some research [78], [115]–[117], [121] explores to pass the generated images through an inverse network to yield the conditional input, which imposes a cycle-consistency of conditional input. The inverse network varies for different conditional inputs, *e.g.*, image captioning models [78], [122] for text guidance, generation networks for visual guidance.

Loss Design. Except for the inherent adversarial loss in GANs, various other loss terms have been explored to achieve high-fidelity generation or faithful conditional generation. For conditional input that is spatially aligned with the ground-truth image, it has been proved that perceptual loss [123] is able to boost the generation quality significantly [124], by minimizing the distance of perceptual features between generated images and the ground-truth. Besides, associated with the cycle structure described previously, a cycle-consistency loss [121] is duly imposed to enforce condition consistency. However, cycle-consistency loss is too restrictive for conditional generation as it assumes a bijective relationship between two domains. Thus, some efforts [120], [125], [126] have been devoted to exploring one-way translation and bypass the bijection constraint of cycle-consistency. With the emergence of contrastive learning, several studies explore to maximize the mutual information of positive pairs via noise contrastive estimation [127] for the preservation of contents in unpaired image generation from visual guidance [128], [129] or text-to-image generation [130]. Except for contrastive loss, triplet loss also has been

employed to improve the condition consistency for cross-modal guidance like texts [113].

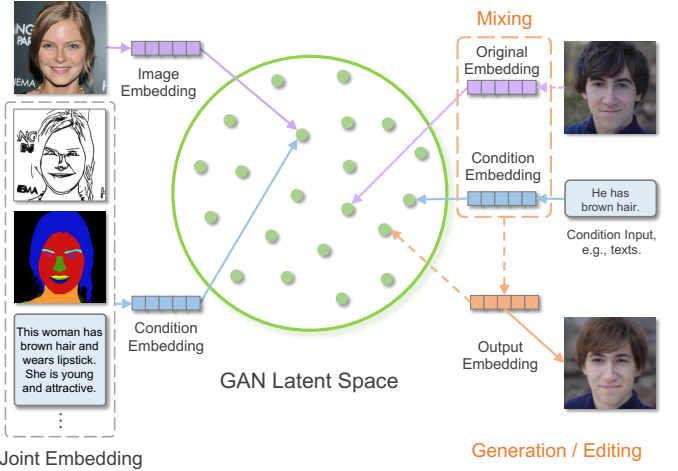


Fig. 4. GAN inversion method with cross-modal alignment in latent space: Both image and condition are embedded into the latent space of GAN (*e.g.*, StyleGAN [18]). The cross-modal similarity learning aims to pull the image embedding and condition embedding to be closer. Then the image embedding and condition embedding can be mixed to perform multimodal image generation or editing via the latent space of GAN. The illustration is reproduced based on [24].

3.1.2 Inversion of Unconditional GAN

Large scale GANs [17], [18] have achieved remarkable progress in unconditional image synthesis with high-resolution and high-fidelity. With a pre-trained GAN model, a series of studies explore to invert a given image back into the latent space of the GAN, which is termed as GAN inversion [22]¹. Specifically, a pre-trained GAN learns a mapping from latent codes to real images, while the GAN inversion maps images back to latent codes, which is achieved by feeding the latent code into the pre-trained GAN to reconstruct the image through optimization. Typically, the reconstruction metrics are based on ℓ_1 , ℓ_2 , perceptual [123] loss or LPIPS [132]. Certain constraints on face identity [133] or latent codes [23] could also be included during optimization. With the obtained latent codes, we can faithfully reconstruct the original image and conduct

1. Please refer to [22] for a comprehensive review of GAN inversion.

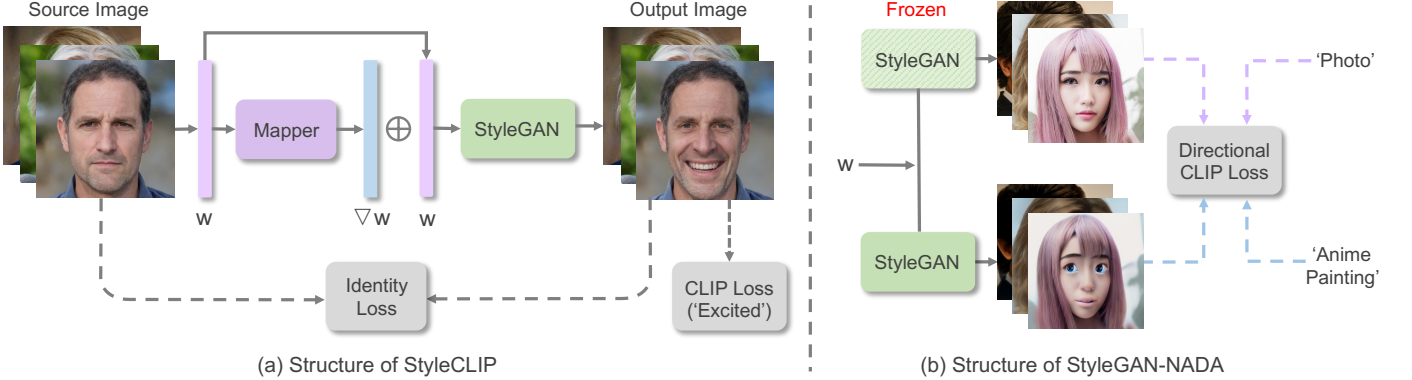


Fig. 5. The architectures of GAN inversion with cross-model supervision for MISE, including (a) StyleCLIP [25] and (b) StyleGAN-NADA [131]. StyleCLIP inverts source image into a latent code. A mapper network is trained to produce residuals that are added to the latent code to yield the target code, from which a pre-trained StyleGAN generates an image assessed by the CLIP and identity losses. StyleGAN-NADA directly finetunes the pretrained StyleGAN by a directional CLIP loss which aligns the CLIP-space directions between the source and target text-image pairs. The figure is reproduced based on [25] and [131].

realistic image manipulation in the latent space. In terms of MISE, cross-modal image manipulation can be achieved by manipulating or generating latent codes according to the guidance from other modalities.

Explicit Cross-model Alignment. One direction of leveraging the guidance from other modalities is to map the embeddings of images and cross-modal inputs (e.g., semantic maps, texts) in a common embedding space [24], [134] as shown in Fig. 4. For example, TediGAN [24] trains an encoder for each modality to extract the embeddings and apply similarity loss to map them into the latent space. Afterwards, latent manipulation (e.g., latent mixing [24]) could be performed to edit the image latent codes toward the embeddings of other modalities and achieve cross-modal image manipulation. However, mapping multimodal data into a common space is non-trivial thanks to the heterogeneity across different modalities, which can result in inferior and unfaithful image generation.

Implicit Cross-model Supervision. Instead of explicitly projecting guidance modality into the latent space, another line of research aims to guide the synthesis or editing by defining consistency loss between the generation results and the guiding modality. For instance, Jiang *et al.* [135] propose to optimize image latent codes through a pre-trained fine-grained attribute predictor, which can examine the consistency of the edited image and the text description. However, the attribute predictor is specifically designed for face editing with fine-grained attribute annotations, making it hard to generalize to other scenarios. A recently released large-scale pretrained model, Contrastive Language-Image Pre-training (CLIP) [45] has demonstrated great potential in multimodal synthesis and manipulation [25], [32], which learns joint vision-language representations from over 400M text-image pairs via contrastive learning. On the strength of the powerful pre-trained CLIP, Bau *et al.* [136] define a CLIP-based semantic consistency loss to optimize latent codes inside an inpainting region to align the recovered content with the given text. Similarly, StyleClip [25] and StyleMC [137] employ cosine similarity between CLIP representations to supervise the text-guided manipulation as illustrated in Fig. 5 (a). A known issue of standard CLIP

loss is the adversarial solution [138], where the model tends to fool the CLIP classifier by adding meaningless pixel-level perturbations to the image. To this end, Liu *et al.* propose AugCLIP score [138] to robustify the standard CLIP score; StyleGAN-NADA [131] presents a directional CLIP loss to align the CLIP-space directions between the source and target text-image pairs as shown in Fig. 5 (b). It also directly finetunes the pretrained generative model with text conditions for domain adaptation. Moreover, Yu *et al.* [139] introduce a CLIP-based contrastive loss for robust optimization and counterfactual image manipulation.

3.2 Autoregressive Methods

Fueled by the advance of GPT [27] in natural language modeling, autoregressive models have been successfully applied to image generation [28] by treating the flattened image sequences as discrete tokens. The plausibility of generated images demonstrates that autoregressive models are able to accommodate the spatial relationships between pixels and high-level attributes. As Transformer models are friendly to multimodal inputs, a series of studies have been proposed to explore multimodal image synthesis with Transformer-based autoregressive models [33], [34], [141], [142]. Overall, the pipeline of autoregressive model for MISE consists of a *vector quantization* [31], [143] stage to yield unified discrete representation and achieve data compression, and an *autoregressive modeling* stage which establishes the dependency between discrete tokens in a raster-scan order as illustrated in Fig. 6.

3.2.1 Vector Quantization

Directly treating all image pixels as a sequence for autoregressive modeling with Transformer is expensive in terms of memory consumption as the self-attention mechanism in Transformer incurs quadratic memory cost. Thus, compressed and discrete representation of image is essential and significant for autoregressive image synthesis and editing. A k-means method to cluster RGB pixel values has been adopted in [28] to reduce the input dimensionality. However, k-means clustering only reduces the dimensionality while the sequence length is still unchanged. Thus,

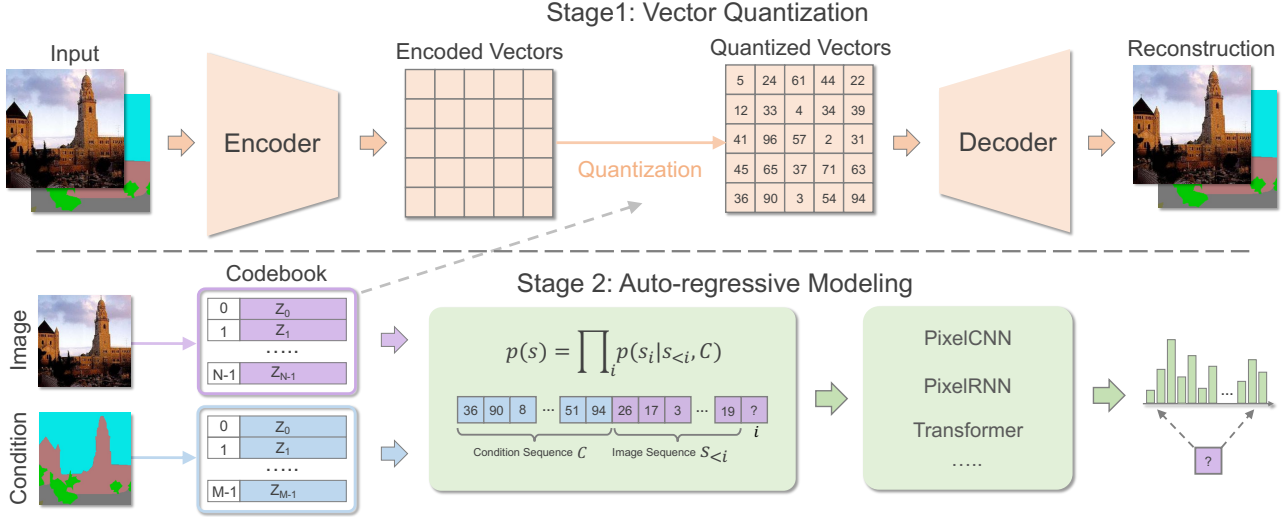


Fig. 6. Typical framework of autoregressive methods for MISE tasks. A quantization stage is firstly performed to learn discrete and compressed representation by reconstructing the original image or condition (e.g., semantic map) faithfully via VQ-GAN [31], [33], followed by an autoregressive modeling stage to capture the dependency of discrete sequence. The image is reproduced based on [33] and [140].

the autoregressive model still cannot be scaled to higher resolutions, due to the quadratically increasing cost in sequence length. To this end, Vector Quantised VAE (VQ-VAE) [31] is adopted to learn discrete and compressed image representation. VQ-VAE consists of an encoder, a feature quantizer, and a decoder. The image is fed into the encoder to learn a continuous representation, which is quantized via the feature quantizer by assigning the feature to the nearest codebook entry. Then the decoder reconstructs the original image from the quantized feature, driving to learn a faithful discrete image representation. As assigning codebook entry is not differentiable, a reparameterization trick [31], [144] is usually adopted to approximate the gradient. Targeting for learning superior discrete image representation, a series of efforts [33], [145], [146] have been devoted to improving VQ-VAE in terms of loss function, model architecture, codebook utilization, and learning regularization.

Loss Function. To achieve desirable perceptual quality for reconstructed images, an adversarial loss and a perceptual loss [123], [147], [148] (with pre-trained VGG) can be incorporated for image reconstruction. With the extra adversarial loss and perceptual loss, the image quality is clearly improved compared with the original pixel loss as validated in [33]. Except for pre-trained VGG for computing perceptual loss, vision Transformer [149] from self-supervised learning [81], [150] is also proved to work well for calculating perceptual loss. Besides, to emphasize reconstruction quality in certain regions, a feature-matching loss can be employed over the activations of certain pre-trained models, *e.g.*, face-embedding network [151] which can improve the reconstruction quality of face region.

Network Architecture. Convolution neural network is the common structure to learn the discrete image representation in VQ-VAE. Recently, Yu *et al.* [145] replace the convolution-based structure with Vision Transformer (ViT) [152], which is shown to be less constrained by the inductive priors imposed by convolutions and is able to yield better computational efficiency with higher reconstruction quality.

With the emergence of diffusion models, diffusion-based decoder [153] also has been explored to learn discrete image representation with superior reconstruction quality. On the other hand, a multi-scale quantization structure is proved to promote the generation performance by including both low-level pixels and high-level tokens [154] or hierarchical latent codes [155]. To further reduce the computational costs, a residual quantization [156] can be employed to recursively quantize the image as a stacked map of discrete tokens.

Codebook Utilization. The vanilla VQ-VAE with argmin operation (to get the nearest codebook entry) suffers from severe codebook collapse, *e.g.*, only few codebook entries are effectively utilized for quantization [157]. To alleviate the codebook collapse, vq-wav2vec [158] introduces Gumbel-Softmax [159] to replace argmin for quantization. The Gumbel-Softmax allows sampling discrete representation in a differentiable way through straight-through gradient estimator [144], which boosts the codebook utilization significantly. ViT-VQGAN [145] also presents a factorized code architecture which introduces a linear projection from the encoder output to a low dimensional latent variable space for code index lookup and boosts the codebook usage substantially.

Learning Regularization. Recent work [146] validates that the vanilla VQ-VAE doesn't satisfy translation equivariance during quantization, resulting in degraded performance for text-to-image generation. A simple but effective TE-VQGAN [146] is thus proposed to achieve translation equivariance by regularizing orthogonality in the codebook embeddings. To regularize the latent structure of heterogeneous domain data in conditional generation, Zhan *et al.* [160] design an Integrated Quantization VAE (IQ-VAE) to penalize the inter-domain discrepancy with intra-domain variations.

3.2.2 Autoregressive Modeling

Autoregressive (AR) modeling is a representative paradigm to accommodate sequence dependencies, complying with

the chain rule of probability. The probability of each token in the sequence is conditioned on all previously predictions, yielding a joint distribution of sequences as the product of conditional distributions: $p(x) = \prod_{t=1}^n p(x_t|x_1, x_2, \dots, x_{t-1}) = \prod_{t=1}^n p(x_t|x_{<t})$. During inference, each token is predicted autoregressively in a raster-scan order. Notably, a sliding-window strategy [33] can be employed to reduce the cost during inference by only utilizing the predictions within a local window. A top- k sampling strategy is adopted to randomly sample from the k most likely next tokens, which naturally enables diverse sampling results. The predicted tokens are then concatenated with the previous sequence as conditions for the prediction of next token. This process repeats iteratively until all the tokens are sampled. Autoregressive models for image synthesis have become increasingly popular due to their ability to generate high-quality, realistic images with a high level of detail. In MISE tasks, autoregressive models generate images pixel-by-pixel based on a conditional probability distribution that takes into account both the previously generated pixels and the given conditioning information, which allows the models to capture the complex dependencies to yield visually consistent images. In recent years, autoregressive models for MISE have been largely fueled by series of designs to be introduced below.

Network Architecture. Early autoregressive models for image generation usually adopt PixelCNN [161] which struggle in modeling long term relationships within an image due to the limited receptive field. With the prevailing of Transformer [26], Transformer-based autoregressive models [162] emerge with enhanced receptive field which allows sequentially predicting each pixel conditioned on previous prediction results. To explore the limits of autoregressive text-to-image synthesis, Parti [163] scales the parameter size of Transformer up to 20B, yielding consistent quality improvements in terms of image quality and text-image alignment. Instead of unidirectionally modeling from condition to image, a bi-directional architecture is also explored in text-to-image synthesis [164], [165], which generates both diverse captions and images.

Bidirectional Context. On the other hand, previous methods incorporate image context in a raster-scan order by attending only to previous generation results. This strategy is unidirectional and suffers from sequential bias as it disregards much context information until autoregression is nearly complete. It also ignores much contextual information in different scales as it only processes the image on a single scale. Grounded in above observations, ImageBART [142] presents a coarse-to-fine approach in a unified framework that addresses the unidirectional bias of autoregressive modeling and the corresponding exposure bias. Specifically, a diffusion process is applied to successively eliminate information, yielding a hierarchy of representations which is further compressed via a multinomial diffusion process [166], [167]. By modeling the Markovian transition autoregressively with attending to the preceding hierarchical state, crucial global context can be leveraged for each individual autoregressive step. As an alternative, bidirectional Transformer is also widely explored to incorporate bidirectional context, accompanied with a Masked Visual Token Modeling (MVTM) [168] or Masked Language

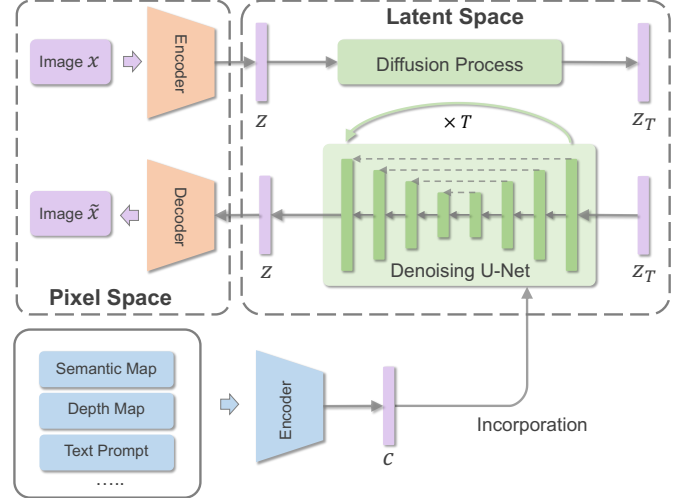


Fig. 7. Overall framework of conditional diffusion model. With a certain model for latent representation, diffusion process models the latent space by reversing a forward diffusion process conditioned on certain guidance (e.g., semantic map, depth map, and texts). The image is reproduced based on [46].

Modeling (MLM) [169], [170] mechanism.

Self-Attention Mechanism. To handle languages, images, and videos in different tasks in a unified manner, NUWA [34] presents a 3D Transformer framework with a unified 3D Nearby Self-Attention (3DNA) which not only reduces the complexity of full attention but also shows superior performance. With a focus on semantic image editing at high resolution, ASSET [171] proposes to sparsify the Transformer’s attention matrix at high resolutions guided by dense attention at lower resolutions, leading to reduced computational cost.

3.3 Diffusion-based Methods

Recently, diffusion models such as denoising diffusion probabilistic models (DDPMs) [167], [172] have achieved great successes in generative image modeling [172]–[175]. DDPMs are a type of latent variable models that consist of a forward diffusion process and a reverse diffusion process. The forward process is a Markov chain where noise is gradually added to the data when sequentially sampling the latent variables \mathbf{x}_t for $t = 1, \dots, T$. Each step in the forward process is a Gaussian transition $q(\mathbf{x}_t|\mathbf{x}_{t-1}) := \mathcal{N}(\sqrt{1 - \beta_t} \mathbf{x}_{t-1}, \beta_t \mathbf{I})$, where $\{\beta_t\}_{t=0}^T$ are fixed or learned variance schedule. The reverse process $q(\mathbf{x}_{t-1}|\mathbf{x}_t)$ is parameterized by another Gaussian transition $p(\mathbf{x}_{t-1}|\mathbf{x}_t) := \mathcal{N}(\mathbf{x}_{t-1}; \mu(\mathbf{x}_t), \sigma_t^2 \mathbf{I})$. $\mu(\mathbf{x}_t)$ can be decomposed into a linear combination of \mathbf{x}_t and a noise approximation model $\epsilon_\theta(\mathbf{x}_t, t)$ that can be learned through optimization. After training $\epsilon(\mathbf{x}, t)$, the sampling process of DDPM can be achieved by following a reverse diffusion process.

Song *et al.* [173] propose an alternative non-Markovian noising process that has the same forward marginals as DDPM but allows using different samplers by changing the variance of the noise. Especially, by setting the noise to 0, which is a DDIM sampling process [173], the sampling process becomes deterministic, enabling full inversion of the latent variables into the original images with signifi-

cantly fewer steps [35], [173]. Notably, the latest work [35] has demonstrated even higher quality of image synthesis performance compared to variational autoencoders (VAEs) [176], flow models [177], [178], autoregressive models [179], [180] and (GANs) [1], [18]. To achieve image generation and editing conditioned on provided guidance, leveraging pre-trained models [39] (by guidance function or fine-tuning) and training conditional models from scratch [46] are both extensively studied in the literature. A downside of guidance function method lies in the requirement of an additional guidance model which leads to a complicated training pipeline. Recently, Ho *et al.* [36] achieve compelling results without a separately guidance model by using a form of guidance that interpolates between predictions from a diffusion model with and without labels. GLIDE [181] compares CLIP-guided diffusion model and conditional diffusion model on text-to-image synthesis task, and concludes that training conditional diffusion model yields better generation performance.

3.3.1 Conditional Diffusion Models

To launch the MISE tasks, a conditional diffusion model can be naturally derived by directly integrating the condition information into the denoising process. Recently, the performance of conditional diffusion models is significantly pushed forward by a series of designs.

Condition Incorporation. As a common framework, a condition-specific encoder is usually employed to project multimodal condition into embedding vectors, which is further incorporated into the model as shown in Fig. 7. The condition-specific encoder can be learned along with the model or directly borrowed from pre-trained models. Typically, CLIP is a common choice for text embedding as adopted in DALL-E 2 [37]. Besides, generic large language models (*e.g.* T5 [183]) pre-trained text corpora also show remarkable effectiveness at encoding text for image synthesis as validated in Imagen [38]. With the condition embedding, diverse mechanisms can be adopted to incorporate it into diffusion models. Specifically, the condition embedding can be naively concatenated or added to the diffusion timestep embedding [35], [184]. In LDM [46], condition embedding is mapped to the intermediate layers of diffusion models via a cross-attention mechanism. Imagen [38] further compares mean pooling and attention pooling with cross attention mechanism and observes both pooling mechanisms perform significantly worse. To fully leverage the conditional information for semantic image synthesis, Wang *et al.* [185] propose to incorporate visual guidance via a spatially-adaptive normalization, which improves both the quality and semantic coherence of generated images. Instead of incorporating condition to train diffusion models from scratch, ControlNet [5] aims to incorporate condition into a pre-trained diffusion model for controllable generation. To preserve production-ready weights of pre-trained models for fast convergence, a ‘zero convolution’ is designed to incorporate the guidance, where the convolution weights are gradually learned from zeros to optimized parameters.

Latent Diffusion. To enable diffusion models training on limited computational resources while retaining their quality and flexibility, several works explore to conduct diffusion process in learned latent spaces [46] as shown in

Fig. 7. Typically, an autoencoding model can be employed to learn a latent space that is perceptually equivalent to the image space. On the other hand, the learned latent spaces may be accompanied with undesired high variance, which highlighting the need for latent space regularizations. As a common choice, KL divergence can be applied to regularize the latent space towards a standard normal distribution. Alternatively, vector quantization can also be applied for regularization via a VQGAN [33] variant with an absorbed quantization layer as in [46]. Besides, VQGAN can directly learn a discrete latent space (quantization layer is not absorbed), which can be modeled by a discrete diffusion process as in VQ-Diffusion [186]. Tang *et al.* [187] further improve VQ-Diffusion by introducing a high-quality inference strategy to alleviate the joint distribution issue.

Model Architecture. Ho *et al.* [172] introduced a U-Net architecture for diffusion models, which can incorporate the inductive bias of CNNs into the diffusion process. This U-Net architecture is further improved by a series of designs, including attention configuration [35], residual block for upsampling and downsampling activations [174], and adaptive group normalization [35]. Although U-Net structure is widely adopted in SOTA diffusion models, Chahal [188] shows that a Transformer-based LDM [46] can yield comparable performance to U-Net-based LDM [46], accompanied with a natural multimodal condition incorporation via multi-head attention. Nevertheless, such Transformer architecture is more favored under the setting of discrete latent space as in [186], [189]. On the other hand, instead of directly generating final images, DALL-E 2 [37] proposes a two-stage structure by producing intermediate image embeddings from text in the CLIP latent space. Then, the image embeddings are applied to condition a diffusion model to generate final images, which allows improving the diversity of generated images [37]. Besides, some other architectures are also explored, including compositional architecture [190] which generates an image by composing a set of diffusion models, multi-diffusion architecture [191] which is composed of multiple diffusion processes with shared parameters or constraints, retrieval-based diffusion model [192] which alleviates the high computational cost, etc.

3.3.2 Pre-trained Diffusion Models

Instead of re-training diffusion models for different conditions which leads to high computational cost, a popular line of research explores to guide the denoising process or fine-tune the weight of pre-trained diffusion models to achieve conditional generation or editing as shown in Fig. 8,

Guidance Function Method. As an early exploration, Dhariwal *et al.* [35] augment pre-trained diffusion models with classifier guidance which can be extended to achieve conditional generation with various guidance. Specifically, the reverse process $p(\mathbf{x}_{t-1}|\mathbf{x}_t)$ with guidance can be rewritten as $p(\mathbf{x}_{t-1}|\mathbf{x}_t, y)$ where y is the provided guidance. Following the derivation in [35], the final diffusion sampling process can be rewritten as:

$$\mathbf{x}_{t-1} = \mu(\mathbf{x}_t) + \sigma_t^2 \nabla_{\mathbf{x}_t} \log p(y|\mathbf{x}_t) + \sigma_t \varepsilon, \quad \varepsilon \sim \mathcal{N}(0, \mathbf{I}) \quad (1)$$

$F(\mathbf{x}_t, y) = \log p(y|\mathbf{x}_t)$ (dubbed as guidance function) indicates the consistency between \mathbf{x}_t and guidance y which

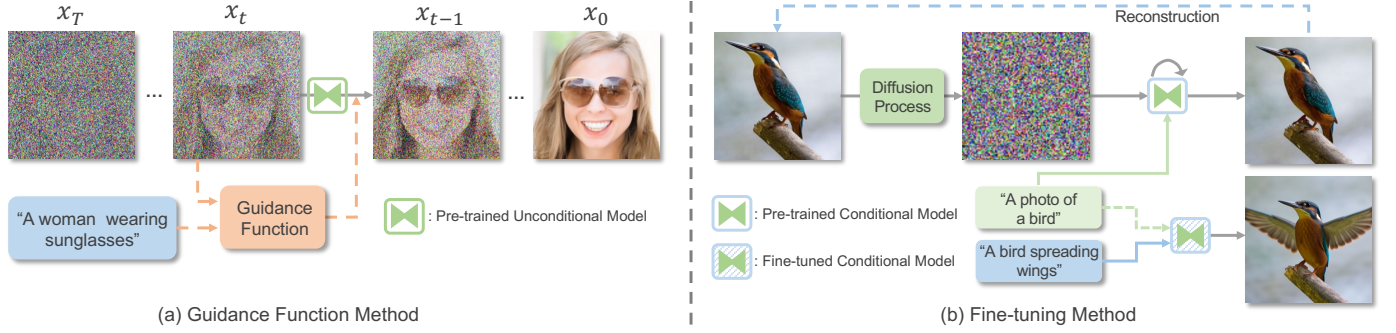


Fig. 8. Typical frameworks of pre-trained diffusion models for MISE tasks, including guidance function method and fine-tuning method. The figure is reproduced based on [39] and [182].

can be formulated by certain similarity metric [39] such as Cosine similarity and L2 distance. As the similarity is usually computed on the feature space, pre-trained CLIP can be adopted as the image encoder and condition encoder for text guidance as shown in Fig. 8 (a). However, the image encoder will take noisy images as input while CLIP is trained on clean images. Thus, a self-supervised fine-tuning of CLIP can be performed to force an alignment between features extracted from clean and noised images as in [39].

To control the generation consistency with the guidance, a parameter γ can be introduced to scale the guidance gradients as below:

$$\mathbf{x}_{t-1} = \mu(\mathbf{x}_t) + \sigma_t^2 \gamma \nabla_{\mathbf{x}_t} \log p(y|\mathbf{x}_t) + \sigma_t \varepsilon, \quad \varepsilon \sim \mathcal{N}(0, \mathbf{I}) \quad (2)$$

Apparently, the model will focus more on the modes of guidance with a larger gradient scale γ . As the result, γ is positively correlated with the generation consistency (with the guidance), while is negatively correlated with the generation diversity [35]. Besides, to achieve the local guidance for image editing, a blended diffusion mechanism [193] can be employed by spatially blending noised image with the local guided diffusion latent at progressive noise levels.

Fine-tuning Method. In terms of fine-tuning, MISE can be achieved by modifying the latent code or adapting the pre-trained diffusion models as shown in Fig. 8 (b). To adapt unconditional pre-trained models for text-guided editing, the input image is first converted to the latent space via the forward diffusion process. The diffusion model at the reverse path is then fine-tuned to generate images driven by the target text and the CLIP loss [40]. For pre-trained conditional models (typically conditioned on texts), similar to GAN Inversion, a text latent embedding or a diffusion model can be fine-tuned to reconstruct a few images (or objects) [42], [43] faithfully. Then the obtained text embedding or fine-tuned model can be applied to generate the same object in novel contexts. However, these methods [42], [43] usually drastically change the layout of the original images. As observing the crux of the relationship between image spatial layout and each word lies in cross-attention layers, Prompt-to-Prompt [41] proposes to preserve some content from the original image by manipulating the cross-attention maps. Alternatively, taking advantage of the step-by-step diffusion sampling process, a model fine-tuned for image reconstruction can be utilized to provide score guidance for content and structure preservation at the early stage

of the denoising process [194]. Similar approach is adopted in [182] by fine-tuning diffusion model and optimizing text embedding via image reconstruction, which allows preserving contents via text embedding interpolation.

3.4 Neural Fields Methods

A neural field [195] is a field that is parameterized fully or in part by a neural network. As a special case of neural fields, Neural Radiance Fields (NeRF) [44] achieve impressive performance for novel views synthesis by parameterizing the color and density of a 3D scene with neural fields. Specifically, a fully-connected neural network is adopted in NeRF, by taking a spatial location (x, y, z) with the corresponding viewing direction (θ, ϕ) as input, and the volume density with the corresponding emitted radiance as output. To render 2D images from the implicit 3D representation, differentiable volume rendering is performed with a numerical integrator [44] to approximate the intractable volumetric projection integral. Powered by NeRF for 3D scene representation, 3D-aware MISE can be achieved with per-scene NeRF or generative NeRF frameworks.

3.4.1 Per-scene NeRF

Consistent with the original NeRF model, a per-scene NeRF aims to optimize and represent a single scene supervised by images or certain pre-trained models.

Image Supervision. With available head pose information and viewing directions, AD-NeRF [8] achieves high-fidelity talking-head synthesis by training neural radiance fields on a video sequence with the audio track of one target person. Instead of bridging audio inputs and video outputs based on the intermediate representations, AD-NeRF directly feeds the audio features into an implicit function to yield a dynamic NeRF, which is further exploited to synthesize high-fidelity talking-face videos accompanied with the audio via volume rendering. However, the paired condition-image data and multiview images are usually unavailable or costly to acquire which hinders the broad applications of this method.

Pre-trained Model Supervision. Instead of relying on multiview images or paired data, certain pre-trained models can be adopted to optimize NeRFs from scratch as shown in Fig. 9 (a). For instance, pre-trained CLIP can be leveraged to achieve text-driven 3D-aware image synthesis [197], by optimizing NeRF to render multi-view images that score highly

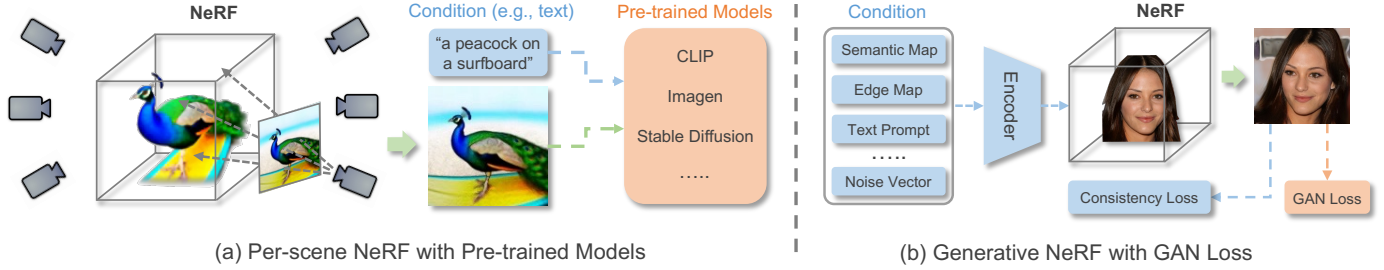


Fig. 9. The frameworks of (a) per-scene NeRF and (b) generative (GAN-based) NeRF for 3D-aware MISE. The image is adapted from [196].

with a target text description according to the CLIP model. Similar CLIP-based approach is also adopted in AvatarCLIP [198] to achieve zero-shot text-driven 3D avatar generation and animation. Recently, with the prosperity of diffusion models, pre-trained 2D diffusion models show great potential to drive the generation of high-fidelity 3D scenes for diverse text prompts as in DreamFusion [196]. Specifically, based on probability density distillation, 2D diffusion model can serve as a generative prior for the optimization of a randomly-initialized 3D neural field via gradient descent such that its 2D renderings yield a high score with the target condition. Following this line of research, Magic3D [199] further proposes to optimize a textured 3D mesh model with an efficient differentiable renderer [200], [201] interacting with a pre-trained latent diffusion model. On the other hand, optimizing NeRF with pre-trained models is an under-constrained process, which highlights the need of certain prior knowledge or regularizations. It has been proved that geometric priors including sparsity regularization and scene bounds [197] improve the generation fidelity significantly. Besides, to mitigate the ambiguous geometry from a single viewpoint, random lighting directions can be applied to shade a scene to reveal the geometric details [196]. To prevent normal vectors from improperly facing backwards from the camera, an orientation loss proposed in Ref-NeRF [202] can be employed to impose penalty.

3.4.2 Generative NeRF

Distinct from per-scene optimization NeRFs which work for a single scene, generative NeRFs are capable of generalizing to different scenes by integrating NeRF with generative models. In generative NeRF, a scene is specified by a latent code in the corresponding latent space. GRAF [203] is the first to introduce a GAN framework for the generative training of radiance fields by employing a multi-scale patch-based discriminator. Lot of efforts have recently been devoted to improve the generative NeRF, *e.g.*, GIRAFFE [204] for introducing volume rendering at the feature level and separating the object instances in a controllable way; PiGAN [205] for the FiLM-based conditioning scheme [206] with a SIREN architecture [207]; StyleNeRF [208] for the integration of style-based generator to achieve high-resolution image synthesis; EG3D [209] for incorporating efficient triplane 3D representation. Fueled by these advancements, 3D-aware MISE can be well performed following the pipeline of conditional generative NeRF or generative NeRF inversion.

Conditional NeRF. In conditional generative NeRF, a scene is specified by the combination of 3D positions and

given conditions as shown in Fig. 9 (b). Recently, Jo *et al.* [210] propose a conditional generative NeRF (CG-NeRF), which can generate multi-view images reflecting extra input conditions (*e.g.*, images or texts). A pre-trained CLIP model is employed to extract the conditional visual and text features to condition a NeRF. Similarly, pix2pix3D [211] encodes certain visual guidance (and a random code) to generate triplanes for scene representation, while it renders the image and pixel-aligned label map simultaneously to enable interactive 3D cross-view editing.

NeRF Inversion. In the light of recent advances in generative NeRFs for 3D-aware image synthesis, some work explores the inversion of generative NeRFs for 3D-aware MISE. As generative NeRF is accompanied with a latent space, the conditional guidance for MISE can be naively mapped into the latent space to enable conditional 3D-aware generation [212]. However, this method struggles for image generation & editing with local control. Some recent work proposes to train 3D-semantic-aware generative NeRF [213], [214] that produces spatial-aligned images and semantic masks concurrently with two branches. These aligned semantic masks can be used to perform local editing of 3D volume via NeRF inversion. On the other hand, the inversion of generative NeRF is challenging due to the including of camera pose. Thus, a hybrid inversion strategy [208] can be applied in practice by combining encoder-based and optimization-based inversion, where the encoder predicts a camera pose and a coarse style code which is further refined through inverse optimization. To enable flexible and faithful 3D-aware MISE, some pre-trained models like CLIP also can be introduced in NeRF inversion. For instance, to achieve 3D-aware manipulation from text prompt, CLIP-NeRF [215] optimizes latent codes towards targeted manipulation driven by a CLIP-based matching loss as described in StyleCLIP [25].

3.5 Other Methods

Except for above-mentioned methods, there has been several endeavors dedicated to the MISE task, exploring diverse research paths.

2D MISE without Generative Models. Instead of relying on generative models, a series of alternative methods have been explored for multimodal editing of 2D images. For instance, CLVA [233] manipulates the style of a content image through text prompts by comparing the contrastive pairs of content image and style instruction to achieve mutual relativity. However, CLVA is constrained as it requires style images accompanied with the text prompts

TABLE 1

Annotation types in popular datasets for MISE. Note, only currently available annotations are labeled with checkmarks, although some off-the-shelf models (e.g., segmentation models, edge detectors, image caption models) can be employed to annotate the corresponding datasets. Part of the information is retrieved from [216].

Datasets	Semantic Map	Keypoint	Sketch	Bounding Box	Depth	Attribute	Text	Audio	Scene Graph
ADE20K [217]	✓	✗	✗	✗	✗	✗	✗	✗	✗
COCO [218]	✓	✓	✗	✓	✗	✗	✓	✗	✗
COCO-Stuff [219]	✓	✗	✗	✗	✗	✗	✗	✗	✓
PSG [220]	✓	✗	✗	✓	✗	✗	✓	✗	✓
Cityscapes [221]	✓	✗	✗	✗	✗	✗	✗	✗	✗
CelebA [222]	✗	✓	✗	✗	✗	✓	✗	✗	✗
CelebA-HQ [119]	✗	✓	✗	✗	✗	✓	✗	✗	✗
CelebAMask-HQ [4]	✓	✓	✗	✗	✗	✓	✗	✗	✗
CelebA-Dialog [135]	✗	✗	✗	✗	✗	✓	✓	✗	✗
MM-CelebA-HQ [24]	✓	✓	✓	✗	✗	✓	✓	✗	✗
DeepFashion [223]	✗	✓	✗	✗	✗	✓	✗	✗	✗
DeepFashion-MM [189]	✓	✓	✗	✗	✗	✓	✓	✗	✗
Chictopia10K [224]	✓	✗	✗	✗	✗	✗	✗	✗	✗
NYU Depth [225]	✓	✗	✗	✗	✓	✗	✗	✗	✗
Stanford’s Cars [226]	✗	✗	✗	✓	✓	✓	✗	✗	✗
Oxford-102 [227]	✗	✗	✗	✗	✗	✓	✓	✗	✗
CUB-200 [228]	✓	✗	✗	✓	✗	✓	✓	✗	✗
LAION-5B [229]	✗	✗	✗	✗	✗	✗	✓	✗	✗
Visual Genome [230]	✗	✗	✗	✓	✗	✓	✓	✗	✓
VoxCeleb [231]	✗	✗	✗	✗	✗	✗	✗	✓	✗
LRS [232]	✗	✗	✗	✗	✗	✗	✓	✓	✗

during training. Instead, CLIPstyler [234] leverages pre-trained CLIP model to achieves text guided style transfer by training a lightweight network which transforms a content image to follow the text condition. As an extension to video, Loeschcke *et al.* [235] harness the power of CLIP to stylize the object in a video according to two target texts.

3D-aware MISE without Neural Fields. Except for neural fields, there are alternative methods that can be leveraged for 3D-aware MISE. Typically, classical 3D representations such as mesh also can be employed to replace neural fields for 3D-aware MISE [236], [237]. Specifically, aiming for style transfer of 3D scenes, Mu *et al.* [238] propose to learn geometry-aware content features from a point cloud representation of the scene, followed by point-to-pixel adaptive attention normalization (AdaAttN) to transfer the style of a given image. Besides, a popular line of research adapts GANs for 3D-aware generation by conditioning on camera parameters [239], introducing intermediate 3D shape [240], incorporating depth prior [241], and adopting 3D rigid-body transformation with projection [242].

3.6 Comparison and Discussion

All generation methods possess their own strength and weakness. GAN-based methods can achieve high-fidelity image synthesis in terms of FID and Inception Score and also have fast inference speed, while GANs are notorious for unstable training and are prone to mode collapse. Moreover, it has been shown that GANs focus more on fidelity rather than capturing the diversity of the training data distribution compared with likelihood-based models like diffusion models and autoregressive models [35]. Besides, GANs usually adopt a CNN architecture (although Transformer structure is explored in some studies [243]–[245]), which makes them struggle to handle multimodal data in a unified manner and generalize to new MISE tasks. With wide adoption of Transformer backbone, autoregressive models can handle different MISE tasks in a unified manner. However, thanks

to the autoregressive prediction of tokens, autoregressive models suffer from slow inference speed, which is also a bottleneck of diffusion models as requiring a number of diffusion steps. Currently, autoregressive models and diffusion models are more favored in SOTA methods compared with GANs, especially for text-to-image synthesis.

Autoregressive models and diffusion models are likely-based generative models which are equipped with stationary training objective and good scalability. The comparison of generative modeling capability between autoregressive models and diffusion is still inconclusive. DALL-E 2 [37] shows that diffusion models are slightly better than autoregressive models in modeling the diffusion prior. However, the recent work Parti [163] which adopts an autoregressive structure presents superior performance over the SOTA work of diffusion-based methods (i.e., Imagen). On the other hand, the exploration of two different families of generative models may open exciting opportunities to combine the merits of the two powerful models.

Different from above generation methods which mainly work on 2D images and have few requirements for the training datasets, NeRF-based methods handle the 3D scene geometry and thus have relatively high requirements for training data. For example, per-scene optimization NeRFs require multiview images with camera pose annotation, while generative NeRFs require the scene geometry of the dataset to be simple. Thus, the application of NeRF in MISE with high-fidelity is still quite constrained. Nevertheless, the 3D-aware modeling of real world with NeRF opens a new door for MISE tasks in the future research.

Besides, state-of-the-art methods are prone to combine different generative models to yield superior performance. For example, Taming Transformer [33] incorporates VQ-GAN and Autoregressive models to achieve high-resolution image synthesis; StyleNeRF [208] combines NeRF with GAN to enable high-fidelity image synthesis with both high-fidelity and 3D-awareness; ImageBart [142] combines the

autoregressive formulation with a multinomial diffusion process to incorporate a coarse-to-fine hierarchy of context information; X-LXMERT [246] integrates GAN into the framework of cross-modality representation to achieve text-guided image generation.

4 EXPERIMENTAL EVALUATION

4.1 Datasets

Datasets are the core of image synthesis and editing tasks. To give an overall picture of the datasets in MISE, we tabulate the detailed annotation types in popular datasets in Table 1. Notably, ADE20K [217], COCO-Stuff [219], and Cityscapes [221] are common benchmark datasets for semantic image synthesis; Oxford-120 Flowers [227], CUB-200 Birds [228], and COCO [218] are widely adopted in text-to-image synthesis; VoxCeleb2 [262] and Lip Reading in the Wild (LRW) [261] are usually used for the benchmark of taking face generation. Please refer to the supplementary material for more details of the widely adopted datasets in different MISE tasks.

4.2 Evaluation Metrics

Precise evaluation metrics are of great importance in driving progress of research. On the other hand, the evaluation of MISE tasks is challenging as multiple attributes account for a fine generation result and the notion of image evaluation is often subjective. To achieve faithful evaluation, comprehensive metrics are adopted to evaluate MISE tasks from multiple aspects. Specifically, Inception Score (IS) [268] and FID [269] are general metrics for image quality evaluation, while LPIPS [132] is a common metric to evaluate image diversity. These metrics can be applied across different generation tasks. In terms of the alignment between generated images and conditions, the evaluation metrics are usually designed for specific generation tasks, e.g., mIoU and mAP for semantic image synthesis, R-precision [77], Captioning Metrics [270] and Semantic Object Accuracy (SOA) [252] for text-to-image generation, cumulative probability blur detection (CPBD) [271] and audio-lip synchronization [272] for talking face generation.

As a general image quality metric, the advantage of the IS is its simplicity, and it can be applied to a wide range of image generation models. However, IS has been criticized for its lack of robustness and sensitivity to noise. It also struggles to evaluate overfitting generation (i.e., the model memorizes the training set) and measure intra-domain variation (i.e., the model only produces one good sample). FID is more robust than the IS and can better capture the overall quality of the generated images. However, it assumes a Gaussian distribution for image features which is not always valid. For diversity evaluation metrics like LPIPS, the quality of generated images is not concerned which means unrealistic generation could lead to a good diversity score. Alignment metric provides quantitative evaluations of generation alignment, while most of them are subject to various issues, including insensitivity to temporal or overall coherence in SOA and CPBD, dataset or pre-trained model bias in R-precision, mIoU & mAP and audio-lip synchronization, ambiguous alignment in Captioning Metrics.

Please refer to the supplementary material for more details of the corresponding evaluation metrics. Overall, certain evaluation metric should be applied in conjunction with other evaluation metrics for a comprehensive and faithful analysis of model performance.

4.3 Experimental Results

We quantitatively compare the image synthesis performance of different models in terms of visual guidance, text guidance, and audio guidance.

4.3.1 Visual Guidance

For visual guidance, we mainly conduct comparison on semantic image synthesis as there are numbers of methods for benchmarking. As shown in Table 2, the experimental comparison is conducted on four challenging datasets: ADE20K [217], ADE20K-outdoors [217], COCO-stuff [219] and Cityscapes [221], following the setting of [3]. The evaluation is performed with FID, LPIPS, and mIoU. Specially, the mIoU aims to assess the alignment between the generated image and the ground truth segmentation via a pre-trained semantic segmentation network. Pre-trained UperNet101 [273], multi-scale DRN-D-105 [274], and DeepLabV2 [275] are adopted for Cityscapes, ADE20K & ADE20K-outdoors, and COCO-Stuff, respectively.

As shown in Table 2, diffusion-based method (i.e., SDM [185]) achieves superior generation quality and diversity as evaluated by FID and LPIPS, and yields comparable semantic consistency as evaluated by mIoU compared with GAN-based methods. Although the comparison may not be fair as the model sizes are different, diffusion-based method still demonstrates its powerful modeling capability for semantic image synthesis. With a large model size, auto-regressive method Taming [33] doesn't show a clear advantage over other methods. We conjecture that Taming Transformer [33] is a versatile framework for various conditional generation tasks without specific design for semantic image synthesis, while other methods in Table 2 mainly focus on the task of semantic image synthesis. Notably, auto-regressive method and diffusion method inherently support diverse conditional generation results, while GAN-based methods usually require additional modules (e.g., Variational Autoencoders (VAEs) [176]) or designs to achieve diverse generation.

4.3.2 Text Guidance

We benchmark text-to-image generation methods on COCO dataset as tabulated in Table 3 (The results are extracted from relevant papers). As shown in Table 3, GAN-based, auto-regressive, and diffusion-based methods can all achieve SOTA performance in terms of FID, e.g., 8.12 in GAN-based method LAFITE [258], 7.23 in auto-regressive method Parti [163], and 7.27 in diffusion-based method Imagen [38]. However, auto-regressive and diffusion-based methods are still preferred in recent SOTA work, thanks to their stationary training objective and good scalability [35].

4.3.3 Audio Guidance

In terms of audio guided image synthesis and editing, we conduct quantitative comparison in the task of audio-driven

TABLE 2
Quantitative comparison with existing methods on segmentation-to-image synthesis. Part of the results are retrieved from [185].

Methods	CelebAMask-HQ			Cityscapes			ADE20K			COCO-Stuff		
	FID ↓	LPIPS ↑	mIoU ↑	FID ↓	LPIPS ↑	mIoU ↑	FID ↓	LPIPS ↑	mIoU ↑	FID ↓	LPIPS ↑	mIoU ↑
Pix2PixHD [118]	38.5	-	76.1	95.0	-	63.0	81.8	-	28.8	111.5	-	26.6
SPADE [3]	29.2	-	75.2	71.8	-	61.2	22.6	-	38.3	33.9	-	38.4
CLADE [247]	30.6	-	75.4	57.2	-	58.6	35.4	-	23.9	29.2	-	38.8
CC-FPSE [248]	-	-	-	54.3	0.026	65.2	31.7	0.078	40.6	19.2	0.098	42.9
GroupDNet [249]	25.9	0.365	76.1	47.3	0.101	55.3	41.7	0.230	27.6	-	-	-
INADE [250]	21.5	0.415	74.1	44.3	0.295	57.7	35.2	0.459	33.0	-	-	-
OASIS [251]	-	-	-	47.7	0.327	58.3	28.3	0.286	45.7	17.0	0.328	46.7
Taming [33]	-	-	-	-	-	-	35.5	0.421	-	-	-	-
SDM [185]	18.8	0.422	77.0	42.1	0.362	77.5	27.5	0.524	39.2	15.9	0.518	40.2

TABLE 3

Text-to-Image generation performance on the COCO dataset. [†] denotes the results obtained by using the corresponding open-source code. The rows in grey and cyan denote the results of Transformer-based and Diffusion-based methods, respectively. Others are the results of GAN-based methods. Part of the results are retrieved from [73].

Methods	IS ↑	FID ↓	R-Prec. ↑
Real Images [252]	34.88	6.09	68.58
StackGAN [70]	8.450	74.05	-
StackGAN++ [71]	8.300	81.59	-
AttnGAN [77]	25.89	35.20	85.47
MirrorGAN [78]	26.47	-	74.52
AttnGAN+OP [252]	24.76	33.35	82.44
OP-GAN [252]	27.88	24.70	89.01
SEGAN [102]	27.86	32.28	-
ControlGAN [103]	24.06	-	82.43
DM-GAN [104]	30.49	32.64	88.56
DM-GAN [104] [†]	32.43	24.24	92.23
Obj-GAN [253]	27.37	25.64	91.05
Obj-GAN [253] [†]	27.32	24.70	91.91
TVBi-GAN [254]	31.01	31.97	-
Wang et al. [255]	29.03	16.28	82.70
Rombach et al. [256]	34.70	30.63	-
CPGAN [257]	52.73	-	93.59
Pavllo et al. [80]	-	19.65	-
XMC-GAN [130]	30.45	9.330	-
LAFITE [258]	32.34	8.120	-
CogView [141]	18.20	27.10	-
CogView2 [259]	22.40	24.10	-
DALL-E [32]	17.90	27.50	-
NUWA [34]	27.20	12.90	-
DiVAE [153]	-	11.53	-
Make-A-Scene [260]	-	11.84	-
Parti [163]	-	7.230	-
VQ-Diffusion [186]	-	13.86	-
LDM [46]	30.29	12.63	-
GLIDE [181]	-	12.24	-
DALL-E 2 [37]	-	10.39	-
Imagen [38]	-	7.270	-

talking face generation which has been widely explored in the literature. Notably, current development of talking face generation mainly relies on GANs, while auto-regressive or diffusion-based methods for talking face generation remain under-explored. The quantitative results of talking face generation on LFW [261] and VoxCeleb2 [262] datasets are shown in Table 4.

5 OPEN CHALLENGES & DISCUSSION

Though MISE has made notable progress and achieved superior performance in recent years, there exist several challenges for future exploration. In this section, we overview the typical challenges, share our humble opinions on possible solutions, and highlight the future research directions.

5.1 Towards Large-Scale Multi-Modality Datasets

As current datasets mainly provide annotations in a single modality (e.g., visual guidance), most existing methods focus on image synthesis and editing conditioned on guidance from a single modality (e.g., text-to-image synthesis, semantic image synthesis). However, humans possess the capability of creating visual contents with guidance of multiple modalities concurrently. Targeting to mimic the human intelligence, multimodal inputs are expected to be fused and leveraged jointly in image generation. Recently, Make-A-Scene [260] explores to include semantic segmentation tokens in auto-regressive modeling to achieve better quality in image synthesis; ControlNet [5] incorporates various visual conditions into Stable Diffusion (for text-to-image generation) to achieve controllable generation; with MM-CelebA-HQ [24], COCO [218], and COCO-Stuff [219] as the training set, PoE-GAN [276] achieves image generation conditioned on multi-modal including segmentation, sketch, image, and text. However, the size of MM-CelebA-HQ [24], COCO [218], and COCO-Stuff [219] is still far from narrowing the gap with real-world distributions. Thus, to incorporate comprehensive modalities into image generation, a natural scene dataset which is equipped with annotations from a wide spectrum of modalities (e.g., semantic segmentation, text description, scene graph) is expected to be created and made publicly available in the future.

5.2 Towards Faithful Evaluation Metrics

The evaluation of MISE is still an open problem. Leveraging pre-trained models to conduct evaluations (e.g., FID) is constrained to the pre-trained datasets, which tends to pose discrepancy with the target datasets. User study recruits human subjects to assess the synthesized images directly, which is however often subjective. Designing accurate yet faithful evaluation metrics is thus very meaningful and critical to the development of multimodal image synthesis and editing.

TABLE 4

The audio guided image editing (talking-head) performance on LWR [261] and VoxCeleb2 [262] under four metrics. \dagger denotes that the model is evaluated by directly using the authors' generated samples under their setting. Part of the results are retrieved from [96].

Methods	LRW [261]				VoxCeleb2 [262]			
	SSIM \uparrow	CPBD \uparrow	LMD \downarrow	Sync _{conf} \uparrow	SSIM \uparrow	CPBD \uparrow	LMD \downarrow	Sync _{conf} \uparrow
ATVG [105]	0.810	0.102	5.25	4.1	0.826	0.061	6.49	4.3
Wav2Lip [263]	0.862	0.152	5.73	6.9	0.846	0.078	12.26	4.5
MakeItTalk [106]	0.796	0.161	7.13	3.1	0.817	0.068	31.44	2.8
Rhythmic Head \dagger [108]	-	-	-	-	0.779	0.802	14.76	3.8
PC-AVS [96] (Fix Pose)	0.815	0.180	6.14	6.3	0.820	0.084	7.68	5.8
PC-AVS [96]	0.861	0.185	3.93	6.4	0.886	0.083	6.88	5.9
GC-AVT [264]	-	-	-	-	0.710	-	3.03	5.3
EAMM [265]	0.740	-	2.08	5.5	-	-	-	-
SyncTalkFace [266]	0.893	-	1.25	-	-	-	-	-
AVCT [267]	-	-	-	-	-	0.564	0.525	6.98
Ground Truth	1.000	0.173	0.00	6.5	1.000	0.090	0.00	5.9

Recently, to evaluate the cross-modal alignment in text-to-image synthesis, pre-trained CLIP has been used to measure the similarity between the texts and the corresponding generated images. Notably, current advance in multimodal learning [277] enables a more accurate cross-modal coherence, which may contribute to the future development of faithful evaluation metrics.

5.3 Towards Efficient Network Architecture

With inherent support for multimodal input and powerful generative modeling, auto-regressive models and diffusion models have been a new paradigm for unified MISE. However, both auto-regressive models and diffusion models suffer from slow inference speed, which is more severe in high-resolution image synthesis. Some recent work [278], [279] explores to accelerate auto-regressive models and diffusion models, while the experiments are constrained to toy datasets with low resolution like CIFAR-10 [280]. How to accelerate the inference speed of auto-regressive models and diffusion models for practical applications remains a grand challenge for future exploration.

On the other hand, GAN-based methods have a better inference speed while the widely adopted CNN architecture hinders it from unified handling of multimodal inputs. Recently, some work [281], [282] has explored to adopt Transformer-based architecture in GANs, which may provide some insights into developing GANs for unified handling of MISE tasks.

5.4 Towards 3D Awareness

With the emergence of neural scene representation models especially NeRF, 3D-aware image synthesis and editing has the potential to be the next breaking point for MISE as it models the 3D geometry of real world. With the incorporation of adversarial loss, generative NeRF is notably appealing for MISE as it is associated with a latent space. Current generative NeRF models (e.g., StyleNeRF, EG3D) have enabled to model scenes with simple geometry (e.g., faces, cars) from a collection of unposed 2D images, just like the training of unconditional GANs (e.g., StyleGAN). Powered by these efforts, several 3D-aware MISE tasks have been explored, e.g., text-to-NeRF [210] and semantic-to-NeRF [212]. However, current generative NeRFs still struggle on datasets with complex geometry variation, e.g., DeepFashion [223] and ImageNet [283].

Only relying on adversarial loss to learn the complex scene geometry from unposed 2D images is indeed intractable and challenging. A possible solution is to provide more prior knowledge of the scene, e.g., obtaining prior scene geometry or prior with off-the-shelf models [284], providing skeleton prior for generative human modeling, etc. Notably, the power of prior knowledge has been explored in some recent studies of 3D-aware tasks [238], [284], [285]. Another possible approach is to provide more supervision, e.g., creating a large dataset with multiview annotations or geometry information. Once the 3D-aware generative modeling succeeds to work on complex natural scenes, some interesting multimodal applications will become possible, e.g., 3D version of DALL-E.

6 SOCIAL IMPACTS

As related to the hot concept of **AI-Generated Content (AIGC)**, MISE has gained considerable attention in recent years. The rapid advancements in MISE offer unprecedented generation realism and editing possibilities, which have influenced and will continue to influence our society in both positive and potentially negative ways. In this section, we discuss the correlation between MISE and AIGC, and analyze the potential social impacts of MISE.

6.1 Correlation with AIGC

Recently, AI-generated content has been a very hot research topic with emergence of Stable Diffusion² and ChatGPT³. MISE is related to AIGC in that they both involve using machine learning & deep learning to create new and novel visual contents. Nevertheless, MISE is a specific application of AI that focuses on generating & editing images with specific attributes which is controlled by various multimodal guidance. It aims to mimic the visual imaging capability of humans in the multimodal real world. As a comparison, AIGC encompasses a much broader range of creative work including visual contents, text contents, audio contents, etc.

6.2 Applications

The multi-modal image synthesis and editing techniques can be applied in artistic creation and content generation,

2. <https://stablediffusionweb.com>

3. <https://openai.com/blog/chatgpt>

which could widely benefit designers, photographers, and content creators [286]. Moreover, they can be democratized in everyday applications as image generation or editing tools for popular entertainment. In addition, the various conditions as intermediate representations for synthesis & editing greatly ease the use of the methods and improve the flexibility of user interaction. In general, the techniques greatly lower the barrier for the public and unleash their creativity on content generation and editing.

6.3 Misuse

On the other hand, the increasing editing capability and generation realism also offers opportunities to generate or manipulate images for malicious purposes. The misuse of synthesis & editing techniques may spread fake or nefarious information and lead to negative social impacts. To prevent potential misuses, one possible way is to develop detection techniques for automatically identifying generated images, which has been actively researched by the community [287]. Meanwhile, sufficient guardrails, labelling, and access control should be carefully considered when deploying MISE techniques to minimize the risk of misuses.

6.4 Environment

As deep-learning-based methods, the current multi-model generative methods inevitably require GPUs and considerable energy consumption for training and inference, which may negatively influence the environment and global climate before the large-scale use of renewable energy. One direction to soften the need for computational resources lies in the active exploration of model generalization. For example, a pretrained model generalized in various datasets could greatly accelerate the training process or provide semantical knowledge for downstream tasks.

7 CONCLUSION

This review has covered main approaches for multimodal image synthesis and editing. Specifically, we provide an overview of different guidance modalities including visual guidance, text guidance, audio guidance, and other modality guidance (e.g., scene graph). In addition, we provided a detailed introduction of the main image synthesis & editing paradigms: GAN-based methods, Autoregressive methods, Diffusion-based methods, and Neural Fields methods. The corresponding strengths and weaknesses were comprehensively discussed to inspire new paradigm that takes advantage of the strengths of existing frameworks. We also conduct a comprehensive survey of datasets and evaluation metrics for MISE conditioned on different guidance modalities. Further, we tabularize and compare the performance of existing approaches in different MISE tasks. Last but not least, we provided our perspective on the current challenges and future directions related to integrating all modalities, comprehensive datasets, evaluation metrics, model architecture, and 3D awareness.

ACKNOWLEDGMENTS

This study is supported under the RIE2020 Industry Alignment Fund – Industry Collaboration Projects (IAF-ICP) Funding Initiative, as well as cash and in-kind contribution from the industry partner(s).

REFERENCES

- [1] I. Goodfellow et al. Generative adversarial nets. *NeurIPS*, 27, 2014.
- [2] P. Isola et al. Image-to-image translation with conditional adversarial networks. In *CVPR*, pp. 1125–1134, 2017.
- [3] T. Park et al. Semantic image synthesis with spatially-adaptive normalization. In *CVPR*, pp. 2337–2346, 2019.
- [4] C.-H. Lee et al. Maskgan: Towards diverse and interactive facial image manipulation. In *CVPR*, pp. 5549–5558, 2020.
- [5] L. Zhang and M. Agrawala. Adding conditional control to text-to-image diffusion models. *arXiv preprint arXiv:2302.05543*, 2023.
- [6] J. Cheng et al. Layoutdiffuse: Adapting foundational diffusion models for layout-to-image generation. *arXiv preprint arXiv:2302.08908*, 2023.
- [7] F. Zhan et al. Unbalanced feature transport for exemplar-based image translation. In *CVPR*, 2021.
- [8] Y. Guo et al. Ad-nerf: Audio driven neural radiance fields for talking head synthesis. In *CVPR*, pp. 5784–5794, 2021.
- [9] Y. Li et al. Pastegan: A semi-parametric method to generate image from scene graph. *NeurIPS*, 32, 2019.
- [10] E. Mansimov et al. Generating images from captions with attention. *arXiv:1511.02793*, 2015.
- [11] M. Mirza and S. Osindero. Conditional generative adversarial nets. *arXiv:1411.1784*, 2014.
- [12] M. Arjovsky et al. Wasserstein generative adversarial networks. In *ICML*, pp. 214–223, 2017.
- [13] C.-H. Lin et al. St-gan: Spatial transformer generative adversarial networks for image compositing. In *CVPR*, pp. 9455–9464, 2018.
- [14] F. Zhan et al. Ga-dan: Geometry-aware domain adaptation network for scene text detection and recognition. In *ICCV*, pp. 9105–9115, 2019.
- [15] A. Shrivastava et al. Learning from simulated and unsupervised images through adversarial training. In *CVPR*, pp. 2107–2116, 2017.
- [16] J. S. Chung et al. You said that? *arXiv:1705.02966*, 2017.
- [17] A. Brock et al. Large scale gan training for high fidelity natural image synthesis. *arXiv:1809.11096*, 2018.
- [18] T. Karras et al. A style-based generator architecture for generative adversarial networks. In *CVPR*, pp. 4401–4410, 2019.
- [19] T. Karras et al. Analyzing and improving the image quality of stylegan. In *CVPR*, pp. 8110–8119, 2020.
- [20] T. Karras et al. Alias-free generative adversarial networks. In *NeurIPS*, 2021.
- [21] L. Goetschalckx et al. Ganalyze: Toward visual definitions of cognitive image properties. In *ICCV*, pp. 5744–5753, 2019.
- [22] W. Xia et al. Gan inversion: A survey. *TPAMI*, 2022.
- [23] J. Zhu et al. In-domain gan inversion for real image editing. In *ECCV*, pp. 592–608. Springer, 2020.
- [24] W. Xia et al. Tedigan: Text-guided diverse face image generation and manipulation. In *CVPR*, pp. 2256–2265, 2021.
- [25] O. Patashnik et al. Styleclip: Text-driven manipulation of stylegan imagery. In *ICCV*, pp. 2085–2094, 2021.
- [26] A. Vaswani et al. Attention is all you need. In *NeurIPS*, pp. 5998–6008, 2017.
- [27] A. Radford et al. Language models are unsupervised multitask learners. *OpenAI blog*, 1(8):9, 2019.
- [28] M. Chen et al. Generative pretraining from pixels. In *ICML*, pp. 1691–1703. PMLR, 2020.
- [29] P. Dhariwal et al. Jukebox: A generative model for music. *arXiv:2005.00341*, 2020.
- [30] K. Gregor et al. Deep autoregressive networks. In *International Conference on Machine Learning*, pp. 1242–1250. PMLR, 2014.
- [31] A. v. d. Oord et al. Neural discrete representation learning. *arXiv:1711.00937*, 2017.
- [32] A. Ramesh et al. DALL-E: Creating images from text. Technical report, OpenAI, 2021.
- [33] P. Esser et al. Taming transformers for high-resolution image synthesis. *arXiv:2012.09841*, 2020.

[34] C. Wu et al. N\” uwa: Visual synthesis pre-training for neural visual world creation. *arXiv:2111.12417*, 2021.

[35] P. Dhariwal and A. Nichol. Diffusion models beat gans on image synthesis. *NeurIPS*, 2021.

[36] J. Ho and T. Salimans. Classifier-free diffusion guidance. *arXiv:2207.12598*, 2022.

[37] A. Ramesh et al. Hierarchical text-conditional image generation with clip latents. *arXiv:2204.06125*, 2022.

[38] C. Saharia et al. Photorealistic text-to-image diffusion models with deep language understanding. *arXiv:2205.11487*, 2022.

[39] X. Liu et al. More control for free! image synthesis with semantic diffusion guidance. *arXiv:2112.05744*, 2021.

[40] G. Kim and J. C. Ye. Diffusionclip: Text-guided image manipulation using diffusion models. *arXiv:2110.02711*, 2021.

[41] A. Hertz et al. Prompt-to-prompt image editing with cross attention control. *arXiv:2208.01626*, 2022.

[42] N. Ruiz et al. Dreambooth: Fine tuning text-to-image diffusion models for subject-driven generation. *arXiv:2208.12242*, 2022.

[43] R. Gal et al. An image is worth one word: Personalizing text-to-image generation using textual inversion. *arXiv:2208.01618*, 2022.

[44] B. Mildenhall et al. Nerf: Representing scenes as neural radiance fields for view synthesis. In *ECCV*, pp. 405–421. Springer, 2020.

[45] A. Radford et al. Learning transferable visual models from natural language supervision. *arXiv:2103.00020*, 2021.

[46] R. Rombach et al. High-resolution image synthesis with latent diffusion models. In *CVPR*, pp. 10684–10695, 2022.

[47] L. Ma et al. Pose guided person image generation. *arXiv:1705.09368*, 2017.

[48] Y. Men et al. Controllable person image synthesis with attribute-decomposed gan. In *CVPR*, 2020.

[49] C. Zhang et al. Deep monocular 3d human pose estimation via cascaded dimension-lifting. *arXiv:2104.03520*, 2021.

[50] J.-Y. Zhu et al. Toward multimodal image-to-image translation. In *NeurIPS*, pp. 465–476, 2017.

[51] H.-Y. Lee et al. Diverse image-to-image translation via disentangled representations. In *ECCV*, pp. 35–51, 2018.

[52] C. Gao et al. Sketchycoco: Image generation from freehand scene sketches. In *CVPR*, pp. 5174–5183, 2020.

[53] W. Chen and J. Hays. Sketchygan: Towards diverse and realistic sketch to image synthesis. In *CVPR*, pp. 9416–9425, 2018.

[54] S.-Y. Chen et al. Deepfacedrawing: Deep generation of face images from sketches. *TOG*, 2020.

[55] M. Zhu et al. A deep collaborative framework for face photo-sketch synthesis. *TNNLS*, 2019.

[56] M. Zhu et al. Learning deep patch representation for probabilistic graphical model-based face sketch synthesis. *IJCV*, 2021.

[57] M. Zhu et al. Knowledge distillation for face photo-sketch synthesis. *TNNLS*, 2020.

[58] Z. Li et al. Staged sketch-to-image synthesis via semi-supervised generative adversarial networks. *TMM*, 2020.

[59] W. Sun and T. Wu. Image synthesis from reconfigurable layout and style. In *ICCV*, pp. 10531–10540, 2019.

[60] B. Zhao et al. Image generation from layout. In *CVPR*, pp. 8584–8593, 2019.

[61] Y. Li et al. Bachgan: High-resolution image synthesis from salient object layout. In *CVPR*, 2020.

[62] Z. Li et al. Image synthesis from layout with locality-aware mask adaption. In *ICCV*, pp. 13819–13828, 2021.

[63] S. Frolov et al. Attrlostgan: Attribute controlled image synthesis from reconfigurable layout and style. *arXiv:2103.13722*, 2021.

[64] J. Y. Koh et al. Text-to-image generation grounded by fine-grained user attention. In *WACV*, pp. 237–246, 2021.

[65] T. Sun et al. Single image portrait relighting. *TOG*, 2019.

[66] P. P. Srinivasan et al. Nerv: Neural reflectance and visibility fields for relighting and view synthesis. In *CVPR*, 2021.

[67] F. Zhan et al. Emlight: Lighting estimation via spherical distribution approximation. In *AAAI*, 2021.

[68] F. Zhan et al. Bi-level feature alignment for versatile image translation and manipulation. In *ECCV*, 2022.

[69] H. Zheng et al. Semantic layout manipulation with high-resolution sparse attention. *TPAMI*, 2022.

[70] H. Zhang et al. StackGAN: Text to photo-realistic image synthesis with stacked generative adversarial networks. In *ICCV*, 2017.

[71] H. Zhang et al. Stackgan++: Realistic image synthesis with stacked generative adversarial networks. *TPAMI*, 2018.

[72] S. Reed et al. Generative adversarial text to image synthesis. In *ICML*, pp. 1060–1069. PMLR, 2016.

[73] S. Frolov et al. Adversarial text-to-image synthesis: A review. *NN*, 2021.

[74] Y. Yang et al. Multi-sentence auxiliary adversarial networks for fine-grained text-to-image synthesis. *TIP*, 2021.

[75] T. Mikolov et al. Distributed representations of words and phrases and their compositionality. In *NeurIPS*, pp. 3111–3119, 2013.

[76] Z. S. Harris. Distributional structure. *Word*, 1954.

[77] T. Xu et al. Attngan: Fine-grained text to image generation with attentional generative adversarial networks. In *CVPR*, pp. 1316–1324, 2018.

[78] T. Qiao et al. Mirrorgan: Learning text-to-image generation by redescription. In *CVPR*, pp. 1505–1514, 2019.

[79] T. Wang et al. Faces à la carte: Text-to-face generation via attribute disentanglement. In *WACV*, pp. 3380–3388, 2021.

[80] D. Pavllo et al. Controlling style and semantics in weakly-supervised image generation. In *ECCV*, pp. 482–499. Springer, 2020.

[81] J. Devlin et al. Bert: Pre-training of deep bidirectional transformers for language understanding. *arXiv:1810.04805*, 2018.

[82] D. Harwath and J. R. Glass. Learning word-like units from joint audio-visual analysis. *arXiv:1701.07481*, 2017.

[83] D. Harwath et al. Vision as an interlingua: Learning multilingual semantic embeddings of untranscribed speech. In *2018 IEEE International Conference on Acoustics, Speech and Signal Processing (ICASSP)*, pp. 4969–4973. IEEE, 2018.

[84] J. Li et al. Direct speech-to-image translation. *JSTSP*, 2020.

[85] Y. Aytar et al. Soundnet: Learning sound representations from unlabeled video. *NeurIPS*, 29:892–900, 2016.

[86] S. Hochreiter and J. Schmidhuber. Long short-term memory. *Neural computation*, 1997.

[87] A. Owens et al. Visually indicated sounds. In *CVPR*, pp. 2405–2413, 2016.

[88] Y. Song et al. Talking face generation by conditional recurrent adversarial network. *arXiv:1804.04786*, 2018.

[89] P. Ekman et al. Facial action coding system (facs) a human face. *Salt Lake City*, 2002.

[90] J. Johnson et al. Image generation from scene graphs. In *CVPR*, pp. 1219–1228, 2018.

[91] D. M. Vo and A. Sugimoto. Visual-relation conscious image generation from structured-text. In *ECCV*, pp. 290–306. Springer, 2020.

[92] X. Shi et al. Convolutional lstm network: A machine learning approach for precipitation nowcasting. *NeurIPS*, 28, 2015.

[93] T. Fang et al. Reconstructing perceptive images from brain activity by shape-semantic gan. *NeurIPS*, 33:13038–13048, 2020.

[94] S. Lin et al. Mind reader: Reconstructing complex images from brain activities. *arXiv preprint arXiv:2210.01769*, 2022.

[95] Y. Takagi and S. Nishimoto. High-resolution image reconstruction with latent diffusion models from human brain activity. *bioRxiv*, pp. 2022–11, 2022.

[96] H. Zhou et al. Pose-controllable talking face generation by implicitly modularized audio-visual representation. In *CVPR*, pp. 4176–4186, 2021.

[97] H. Tang et al. Multi-channel attention selection gan with cascaded semantic guidance for cross-view image translation. In *CVPR*, pp. 2417–2426, 2019.

[98] P. Zhang et al. Cross-domain correspondence learning for exemplar-based image translation. In *CVPR*, pp. 5143–5153, 2020.

[99] X. Zhou et al. Cocosnet v2: Full-resolution correspondence learning for image translation. In *CVPR*, pp. 11465–11475, 2021.

[100] P. Zhu et al. Sean: Image synthesis with semantic region-adaptive normalization. In *CVPR*, June 2020.

[101] W. Huang et al. Realistic image generation using region-phrase attention. In *ACML*, pp. 284–299, 2019.

[102] H. Tan et al. Semantics-enhanced adversarial nets for text-to-image synthesis. In *ICCV*, pp. 10501–10510, 2019.

[103] B. Li et al. Controllable text-to-image generation. *arXiv:1909.07083*, 2019.

[104] M. Zhu et al. Dm-gan: Dynamic memory generative adversarial networks for text-to-image synthesis. In *CVPR*, pp. 5802–5810, 2019.

[105] L. Chen et al. Hierarchical cross-modal talking face generation with dynamic pixel-wise loss. In *CVPR*, pp. 7832–7841, 2019.

[106] Y. Zhou et al. Makeltalk: speaker-aware talking-head animation. *TOG*, 2020.

- [107] V. Blanz et al. A morphable model for the synthesis of 3d faces. In *Siggraph*, pp. 187–194, 1999.
- [108] L. Chen et al. Talking-head generation with rhythmic head motion. In *ECCV*, pp. 35–51. Springer, 2020.
- [109] H. Zhou et al. Talking face generation by adversarially disentangled audio-visual representation. In *AAAI*, pp. 9299–9306, 2019.
- [110] S. Suwajanakorn et al. Synthesizing obama: learning lip sync from audio. *TOG*, 2017.
- [111] S. Wang et al. One-shot talking face generation from single-speaker audio-visual correlation learning. *arXiv:2112.02749*, 2021.
- [112] Z. Zhang et al. Photographic text-to-image synthesis with a hierarchically-nested adversarial network. In *CVPR*, pp. 6199–6208, 2018.
- [113] G. Yin et al. Semantics disentangling for text-to-image generation. In *CVPR*, pp. 2327–2336, 2019.
- [114] M. Cha et al. Adversarial learning of semantic relevance in text to image synthesis. In *AAAI*, pp. 3272–3279, 2019.
- [115] H. Tang et al. Cycle in cycle generative adversarial networks for keypoint-guided image generation. In *MM*, pp. 2052–2060, 2019.
- [116] Q. Lao et al. Dual adversarial inference for text-to-image synthesis. In *ICCV*, pp. 7567–7576, 2019.
- [117] Z. Chen and Y. Luo. Cycle-consistent diverse image synthesis from natural language. In *ICMEW*, pp. 459–464. IEEE, 2019.
- [118] T.-C. Wang et al. High-resolution image synthesis and semantic manipulation with conditional gans. In *CVPR*, pp. 8798–8807, 2018.
- [119] T. Karras et al. Progressive growing of gans for improved quality, stability, and variation. *arXiv:1710.10196*, 2017.
- [120] M. Amadio and S. Krishnaswamy. Travelgan: Image-to-image translation by transformation vector learning. In *CVPR*, pp. 8983–8992, 2019.
- [121] J.-Y. Zhu et al. Unpaired image-to-image translation using cycle-consistent adversarial networks. In *ICCV*, pp. 2223–2232, 2017.
- [122] A. Nguyen et al. Plug & play generative networks: Conditional iterative generation of images in latent space. In *CVPR*, pp. 4467–4477, 2017.
- [123] J. Johnson et al. Perceptual losses for real-time style transfer and super-resolution. In *ECCV*, pp. 694–711. Springer, 2016.
- [124] C. Wang et al. Perceptual adversarial networks for image-to-image transformation. *IEEE Transactions on Image Processing*, 2018.
- [125] S. Benaim and L. Wolf. One-sided unsupervised domain mapping. *NeurIPS*, 30, 2017.
- [126] H. Fu et al. Geometry-consistent generative adversarial networks for one-sided unsupervised domain mapping. In *CVPR*, pp. 2427–2436, 2019.
- [127] A. v. d. Oord et al. Representation learning with contrastive predictive coding. *arXiv:1807.03748*, 2018.
- [128] T. Park et al. Contrastive learning for unpaired image-to-image translation. In *ECCV*, pp. 319–345. Springer, 2020.
- [129] A. Andonian et al. Contrastive feature loss for image prediction. In *ICCV*, pp. 1934–1943, 2021.
- [130] H. Zhang et al. Cross-modal contrastive learning for text-to-image generation. In *CVPR*, pp. 833–842, 2021.
- [131] R. Gal et al. Stylegan-nada: Clip-guided domain adaptation of image generators. *arXiv:2108.00946*, 2021.
- [132] R. Zhang et al. The unreasonable effectiveness of deep features as a perceptual metric. In *CVPR*, pp. 586–595, 2018.
- [133] E. Richardson et al. Encoding in style: a stylegan encoder for image-to-image translation. *arXiv:2008.00951*, 2020.
- [134] H. Wang et al. Cycle-consistent inverse gan for text-to-image synthesis. In *MM*, pp. 630–638, 2021.
- [135] Y. Jiang et al. Talk-to-edit: Fine-grained facial editing via dialog. In *ICCV*, pp. 13799–13808, 2021.
- [136] D. Bau et al. Paint by word. *arXiv:2103.10951*, 2021.
- [137] U. Kocasari et al. Stylemc: Multi-channel based fast text-guided image generation and manipulation. *arXiv:2112.08493*, 2021.
- [138] X. Liu et al. Fusedream: Training-free text-to-image generation with improved clip+ gan space optimization. *arXiv:2112.01573*, 2021.
- [139] Y. Yu et al. Towards counterfactual image manipulation via clip. *arXiv:2207.02812*, 2022.
- [140] F. Zhan et al. Auto-regressive image synthesis with integrated quantization. In *ECCV*, pp. 110–127, 2022.
- [141] M. Ding et al. Cogview: Mastering text-to-image generation via transformers. *arXiv:2105.13290*, 2021.
- [142] P. Esser et al. Imagebart: Bidirectional context with multinomial diffusion for autoregressive image synthesis. In *NeurIPS*, 2021.
- [143] J. T. Rolfe. Discrete variational autoencoders. *arXiv:1609.02200*, 2016.
- [144] Y. Bengio et al. Estimating or propagating gradients through stochastic neurons for conditional computation. *arXiv:1308.3432*, 2013.
- [145] J. Yu et al. Vector-quantized image modeling with improved vqgan. *arXiv:2110.04627*, 2021.
- [146] W. Shin et al. Translation-equivariant image quantizer for bi-directional image-text generation. *arXiv:2112.00384*, 2021.
- [147] A. Lamb et al. Discriminative regularization for generative models. *arXiv:1602.03220*, 2016.
- [148] A. B. L. Larsen et al. Autoencoding beyond pixels using a learned similarity metric. In *ICML*, pp. 1558–1566. PMLR, 2016.
- [149] X. Dong et al. Poco: Perceptual codebook for bert pre-training of vision transformers. *arXiv:2111.12710*, 2021.
- [150] H. Bao et al. Beit: Bert pre-training of image transformers. *arXiv:2106.08254*, 2021.
- [151] Q. Cao et al. Vggface2: A dataset for recognising faces across pose and age. In *FG*, pp. 67–74. IEEE, 2018.
- [152] A. Dosovitskiy et al. An image is worth 16x16 words: Transformers for image recognition at scale, 2020.
- [153] J. Shi et al. Divae: Photorealistic images synthesis with denoising diffusion decoder. *arXiv:2206.00386*, 2022.
- [154] M. Ni et al. NÜwa-lip: Language guided image inpainting with defect-free vqgan. *arXiv:2202.05009*, 2022.
- [155] A. Razavi et al. Generating diverse high-fidelity images with vq-vae-2. In *NeurIPS*, 2019.
- [156] D. Lee et al. Autoregressive image generation using residual quantization. In *CVPR*, 2022.
- [157] J. Zhang et al. Regularized vector quantization for tokenized image synthesis. In *CVPR*, 2023.
- [158] A. Baevski et al. vq-wav2vec: Self-supervised learning of discrete speech representations. *arXiv:1910.05453*, 2019.
- [159] E. Jang et al. Categorical reparameterization with gumbel-softmax. *arXiv:1611.01144*, 2016.
- [160] F. Zhan et al. Auto-regressive image synthesis with integrated quantization. In *ECCV*, 2022.
- [161] A. Van den Oord et al. Conditional image generation with pixelcnn decoders. In *NeurIPS*, 2016.
- [162] N. Parmar et al. Image transformer. In *ICML*, 2018.
- [163] J. Yu et al. Scaling autoregressive models for content-rich text-to-image generation. *arXiv:2206.10789*, 2022.
- [164] Y. Huang et al. A picture is worth a thousand words: A unified system for diverse captions and rich images generation. In *MM*, pp. 2792–2794, 2021.
- [165] Y. Huang et al. Unifying multimodal transformer for bi-directional image and text generation. In *MM*, pp. 1138–1147, 2021.
- [166] E. Hoogeboom et al. Argmax flows and multinomial diffusion: Towards non-autoregressive language models. *arXiv:2102.05379*, 2021.
- [167] J. Sohl-Dickstein et al. Deep unsupervised learning using nonequilibrium thermodynamics. In *ICML*, pp. 2256–2265. PMLR, 2015.
- [168] H. Chang et al. Maskgit: Masked generative image transformer. In *CVPR*, pp. 11315–11325, 2022.
- [169] Z. Zhang et al. M6-ufc: Unifying multi-modal controls for conditional image synthesis. *arXiv:2105.14211*, 2021.
- [170] Y. Yu et al. Diverse image inpainting with bidirectional and autoregressive transformers. In *MM*, pp. 69–78, 2021.
- [171] D. Liu et al. Asset: autoregressive semantic scene editing with transformers at high resolutions. *TOG*, 2022.
- [172] J. Ho et al. Denoising diffusion probabilistic models. *NeurIPS*, 33:6840–6851, 2020.
- [173] J. Song et al. Denoising diffusion implicit models. *arXiv:2010.02502*, 2020.
- [174] Y. Song et al. Score-based generative modeling through stochastic differential equations. *arXiv:2011.13456*, 2020.
- [175] A. Jolicoeur-Martineau et al. Adversarial score matching and improved sampling for image generation. *arXiv:2009.05475*, 2020.
- [176] D. P. Kingma and M. Welling. Auto-encoding variational bayes. *arXiv:1312.6114*, 2013.
- [177] D. Rezende and S. Mohamed. Variational inference with normalizing flows. In *ICML*, pp. 1530–1538. PMLR, 2015.
- [178] L. Dinh et al. Density estimation using real nvp. *arXiv:1605.08803*, 2016.

[179] J. Menick and N. Kalchbrenner. Generating high fidelity images with subscale pixel networks and multidimensional upscaling. *arXiv:1812.01608*, 2018.

[180] A. Van Oord et al. Pixel recurrent neural networks. In *ICML*, pp. 1747–1756. PMLR, 2016.

[181] A. Nichol et al. Glide: Towards photorealistic image generation and editing with text-guided diffusion models. *arXiv:2112.10741*, 2021.

[182] B. Kawar et al. Imagic: Text-based real image editing with diffusion models. *arXiv:2210.09276*, 2022.

[183] C. Raffel et al. Exploring the limits of transfer learning with a unified text-to-text transformer. *JMLR*, 21(140):1–67, 2020.

[184] J. Ho et al. Cascaded diffusion models for high fidelity image generation. *JMLR*, 2022.

[185] W. Wang et al. Semantic image synthesis via diffusion models. *arXiv:2207.00050*, 2022.

[186] S. Gu et al. Vector quantized diffusion model for text-to-image synthesis. *arXiv:2111.14822*, 2021.

[187] Z. Tang et al. Improved vector quantized diffusion models. *arXiv:2205.16007*, 2022.

[188] P. Chahal. Exploring transformer backbones for image diffusion models. *arXiv:2212.14678*, 2022.

[189] Y. Jiang et al. Text2human: Text-driven controllable human image generation. *TOG*, 2022.

[190] N. Liu et al. Compositional visual generation with composable diffusion models. *arXiv:2206.01714*, 2022.

[191] O. Bar-Tal et al. Multidiffusion: Fusing diffusion paths for controlled image generation. *arXiv:2302.08113*, 2023.

[192] A. Blattmann et al. Retrieval-augmented diffusion models. *arXiv:2204.11824*, 2022.

[193] O. Avrahami et al. Blended diffusion for text-driven editing of natural images. *arXiv:2111.14818*, 2021.

[194] Z. Zhang et al. Sine: Single image editing with text-to-image diffusion models. *arXiv:2212.04489*, 2022.

[195] Y. Xie et al. Neural fields in visual computing and beyond. In *CGF*. Wiley Online Library, 2022.

[196] B. Poole et al. Dreamfusion: Text-to-3d using 2d diffusion. In *ICLR*, 2023.

[197] A. Jain et al. Zero-shot text-guided object generation with dream fields. In *CVPR*, pp. 867–876, 2022.

[198] F. Hong et al. Avatarclip: Zero-shot text-driven generation and animation of 3d avatars. *TOG*, 2022.

[199] C.-H. Lin et al. Magic3d: High-resolution text-to-3d content creation. *arXiv:2211.10440*, 2022.

[200] T. Shen et al. Deep marching tetrahedra: a hybrid representation for high-resolution 3d shape synthesis. *NeurIPS*, 2021.

[201] J. Gao et al. Get3d: A generative model of high quality 3d textured shapes learned from images. *NeurIPS*, 2022.

[202] D. Verbin et al. Ref-nerf: Structured view-dependent appearance for neural radiance fields. In *CVPR*, pp. 5481–5490. IEEE, 2022.

[203] K. Schwarz et al. Graf: Generative radiance fields for 3d-aware image synthesis. *NeurIPS*, 33:20154–20166, 2020.

[204] M. Niemeyer and A. Geiger. Giraffe: Representing scenes as compositional generative neural feature fields. In *CVPR*, pp. 11453–11464, 2021.

[205] E. R. Chan et al. pi-gan: Periodic implicit generative adversarial networks for 3d-aware image synthesis. In *CVPR*, pp. 5799–5809, 2021.

[206] E. Perez et al. Film: Visual reasoning with a general conditioning layer. In *AAAI*, volume 32, 2018.

[207] V. Sitzmann et al. Implicit neural representations with periodic activation functions. *NeurIPS*, 33:7462–7473, 2020.

[208] J. Gu et al. Stylenet: A style-based 3d-aware generator for high-resolution image synthesis. In *ICLR*, 2022.

[209] E. R. Chan et al. Efficient geometry-aware 3d generative adversarial networks. In *CVPR*, pp. 16123–16133, 2022.

[210] K. Jo et al. Cg-nerf: Conditional generative neural radiance fields. *arXiv:2112.03517*, 2021.

[211] K. Deng et al. 3d-aware conditional image synthesis. In *CVPR*, 2023.

[212] Y. Chen et al. Sem2nerf: Converting single-view semantic masks to neural radiance fields. *arXiv:2203.10821*, 2022.

[213] J. Sun et al. Ide-3d: Interactive disentangled editing for high-resolution 3d-aware portrait synthesis. *arXiv:2205.15517*, 2022.

[214] J. Sun et al. Fenerf: Face editing in neural radiance fields. In *CVPR*, pp. 7672–7682, 2022.

[215] C. Wang et al. Clip-nerf: Text-and-image driven manipulation of neural radiance fields. *arXiv:2112.05139*, 2021.

[216] Y. Xue et al. Deep image synthesis from intuitive user input: A review and perspectives. *CVM*, 2022.

[217] B. Zhou et al. Scene parsing through ade20k dataset. In *CVPR*, pp. 633–641, 2017.

[218] T.-Y. Lin et al. Microsoft coco: Common objects in context. In *ECCV*, pp. 740–755. Springer, 2014.

[219] H. Caesar et al. Coco-stuff: Thing and stuff classes in context. In *CVPR*, pp. 1209–1218, 2018.

[220] J. Yang et al. Panoptic scene graph generation. *arXiv:2207.11247*, 2022.

[221] M. Cordts et al. The cityscapes dataset for semantic urban scene understanding. In *CVPR*, 2016.

[222] Z. Liu et al. Deep learning face attributes in the wild. In *ICCV*, pp. 3730–3738, 2015.

[223] Z. Liu et al. Deepfashion: Powering robust clothes recognition and retrieval with rich annotations. In *CVPR*, pp. 1096–1104, 2016.

[224] X. Liang et al. Deep human parsing with active template regression. *TPAMI*, 2015.

[225] N. Silberman and R. Fergus. Indoor scene segmentation using a structured light sensor. In *ICCV workshops*, pp. 601–608. IEEE, 2011.

[226] J. Krause et al. 3d object representations for fine-grained categorization. In *ICCV workshops*, pp. 554–561, 2013.

[227] M.-E. Nilsback and A. Zisserman. Automated flower classification over a large number of classes. In *ICVGIP*, 2008.

[228] P. Welinder et al. Caltech-ucsd birds 200. *California Institute of Technology*, 2010.

[229] C. Schuhmann et al. Laion-5b: An open large-scale dataset for training next generation image-text models. In *NeurIPS Datasets and Benchmarks Track*, 2022.

[230] R. Krishna et al. Visual genome: Connecting language and vision using crowdsourced dense image annotations. *IJCV*, 2017.

[231] A. Nagrani et al. Voxceleb: a large-scale speaker identification dataset. *arXiv:1706.08612*, 2017.

[232] J. Son Chung et al. Lip reading sentences in the wild. In *CVPR*, pp. 6447–6456, 2017.

[233] T.-J. Fu et al. Language-driven image style transfer. *arXiv:2106.00178*, 2021.

[234] G. Kwon and J. C. Ye. Clipstyler: Image style transfer with a single text condition. *arXiv:2112.00374*, 2021.

[235] S. Loeschke et al. Text-driven stylization of video objects. *arXiv:2206.12396*, 2022.

[236] O. Michel et al. Text2mesh: Text-driven neural stylization for meshes. In *CVPR*, pp. 13492–13502, 2022.

[237] N. Khalid et al. Text to mesh without 3d supervision using limit subdivision. *arXiv:2203.13333*, 2022.

[238] F. Mu et al. 3d photo stylization: Learning to generate stylized novel views from a single image. In *CVPR*, 2022.

[239] A. Noguchi and T. Harada. Rgbd-gan: Unsupervised 3d representation learning from natural image datasets via rgbd image synthesis. *arXiv:1909.12573*, 2019.

[240] J.-Y. Zhu et al. Visual object networks: Image generation with disentangled 3d representations. *NeurIPS*, 2018.

[241] Z. Shi et al. 3d-aware indoor scene synthesis with depth priors. In *ECCV*, 2022.

[242] T. Nguyen-Phuoc et al. Hologan: Unsupervised learning of 3d representations from natural images. In *ICCV*, 2019.

[243] Y. Jiang et al. Transgan: Two pure transformers can make one strong gan, and that can scale up. *NeurIPS*, 34:14745–14758, 2021.

[244] J. Park and Y. Kim. Styleformer: Transformer based generative adversarial networks with style vector. In *CVPR*, 2022.

[245] D. A. Hudson and C. L. Zitnick. Generative adversarial transformers. *ICML*, 2021.

[246] J. Cho et al. X-lxmert: Paint, caption and answer questions with multi-modal transformers. *arXiv:2009.11278*, 2020.

[247] Z. Tan et al. Efficient semantic image synthesis via class-adaptive normalization. *TPAMI*, 2021.

[248] X. Liu et al. Learning to predict layout-to-image conditional convolutions for semantic image synthesis. *arXiv:1910.06809*, 2019.

[249] Z. Zhu et al. Semantically multi-modal image synthesis. In *CVPR*, pp. 5467–5476, 2020.

[250] Z. Tan et al. Diverse semantic image synthesis via probability distribution modeling. In *CVPR*, pp. 7962–7971, 2021.

- [251] V. Sushko et al. You only need adversarial supervision for semantic image synthesis. *arXiv:2012.04781*, 2020.
- [252] T. Hinz et al. Semantic object accuracy for generative text-to-image synthesis. *arXiv:1910.13321*, 2019.
- [253] W. Li et al. Object-driven text-to-image synthesis via adversarial training. In *CVPR*, pp. 12174–12182, 2019.
- [254] Z. Wang et al. Text to image synthesis with bidirectional generative adversarial network. In *ICME*, pp. 1–6. IEEE, 2020.
- [255] M. Wang et al. End-to-end text-to-image synthesis with spatial constraints. *TIST*, 2020.
- [256] R. Rombach et al. Network-to-network translation with conditional invertible neural networks. *arXiv:2005.13580*, 2020.
- [257] J. Liang et al. Cpgan: Content-parsing generative adversarial networks for text-to-image synthesis. In *ECCV*, pp. 491–508. Springer, 2020.
- [258] Y. Zhou et al. Lafite: Towards language-free training for text-to-image generation. *arXiv:2111.13792*, 2021.
- [259] M. Ding et al. Cogview2: Faster and better text-to-image generation via hierarchical transformers. *arXiv:2204.14217*, 2022.
- [260] O. Gafni et al. Make-a-scene: Scene-based text-to-image generation with human priors. *arXiv:2203.13131*, 2022.
- [261] J. S. Chung and A. Zisserman. Lip reading in the wild. In *ACCV*, pp. 87–103. Springer, 2016.
- [262] J. S. Chung et al. Voxceleb2: Deep speaker recognition. *arXiv:1806.05622*, 2018.
- [263] K. Prajwal et al. A lip sync expert is all you need for speech to lip generation in the wild. In *MM*, pp. 484–492, 2020.
- [264] B. Liang et al. Expressive talking head generation with granular audio-visual control. In *CVPR*, pp. 3387–3396, 2022.
- [265] X. Ji et al. Eamm: One-shot emotional talking face via audio-based emotion-aware motion model. *arXiv:2205.15278*, 2022.
- [266] S. J. Park et al. SyncTalkface: Talking face generation with precise lip-syncing via audio-lip memory. In *AAAI*, 2022.
- [267] S. Wang et al. One-shot talking face generation from single-speaker audio-visual correlation learning. In *AAAI*, 2022.
- [268] T. Salimans et al. Improved techniques for training gans. *NeurIPS*, 29:2234–2242, 2016.
- [269] M. Heusel et al. Gans trained by a two time-scale update rule converge to a local nash equilibrium. In *NeurIPS*, 2017.
- [270] S. Hong et al. Inferring semantic layout for hierarchical text-to-image synthesis. In *CVPR*, pp. 7986–7994, 2018.
- [271] N. D. Narvekar and L. J. Karam. A no-reference image blur metric based on the cumulative probability of blur detection (cpbd). *TIP*, 20(9):2678–2683, 2011.
- [272] J. S. Chung and A. Zisserman. Out of time: automated lip sync in the wild. In *ACCV*, pp. 251–263. Springer, 2016.
- [273] T. Xiao et al. Unified perceptual parsing for scene understanding. In *ECCV*, pp. 418–434, 2018.
- [274] F. Yu et al. Dilated residual networks. In *CVPR*, 2017.
- [275] L.-C. Chen et al. Semantic image segmentation with deep convolutional nets and fully connected crfs. *arXiv:1412.7062*, 2014.
- [276] X. Huang et al. Multimodal conditional image synthesis with product-of-experts gans. *arXiv:2112.05130*, 2021.
- [277] J. Summaira et al. Recent advances and trends in multimodal deep learning: A review. *arXiv:2105.11087*, 2021.
- [278] V. Jayaram and J. Thickstun. Parallel and flexible sampling from autoregressive models via langevin dynamics. In *ICML*, pp. 4807–4818. PMLR, 2021.
- [279] T. Dockhorn et al. Score-based generative modeling with critically-damped langevin diffusion. *arXiv:2112.07068*, 2021.
- [280] A. Krizhevsky et al. Learning multiple layers of features from tiny images. *Toronto, ON, Canada*, 2009.
- [281] X. Wang et al. SceneFormer: Indoor scene generation with transformers. *arXiv:2012.09793*, 2020.
- [282] B. Zhang et al. Styleswin: Transformer-based gan for high-resolution image generation. In *CVPR*, pp. 11304–11314, 2022.
- [283] J. Deng et al. ImageNet: A large-scale hierarchical image database. In *CVPR*, 2009.
- [284] I. Skorokhodov et al. 3d generation on imagenet. In *ICLR*, 2023.
- [285] Q. Xu et al. Point-nerf: Point-based neural radiance fields. In *CVPR*, pp. 5438–5448, 2022.
- [286] J. Bailey. The tools of generative art, from flash to neural networks. *Art in America*, 8, 2020.
- [287] Y. Mirsky and W. Lee. The creation and detection of deepfakes: A survey. *CSUR*, 2021.

Fangneng Zhan is a postdoctoral researcher at Max Planck Institute for Informatics. He received the Ph.D. degree in Computer Science & Engineering from Nanyang Technological University. His research interests include generative models and neural rendering. He serves as a reviewer or program committee member for top journals and conferences including TPAMI, ICLR, ICML, NeurIPS, CVPR, ICCV.

Yingchen Yu is currently pursuing the Ph.D. degree at School of Computer Science and Engineering, Nanyang Technological University under Alibaba Talent Programme. His research interests are image synthesis and manipulation.

Rongliang Wu received the Ph.D. degree from School of Computer Science and Engineering, Nanyang Technological University. His research interests include computer vision and deep learning, specifically for facial expression analysis and generation.

Jiahui Zhang is currently pursuing the Ph.D. degree at School of Computer Science and Engineering, Nanyang Technological University. His research interests include computer vision and machine learning.

Shijian Lu is an Associate Professor in the School of Computer Science and Engineering, Nanyang Technological University. He received his PhD in Electrical and Computer Engineering from the National University of Singapore. His research interests include computer vision and deep learning. He has published more than 100 internationally refereed journal and conference papers. Dr Lu is currently an Associate Editor for the journals of Pattern Recognition and Neurocomputing.

Lingjie Liu is the Aravind K. Joshi Assistant Professor in the Department of Computer and Information Science at the University of Pennsylvania. Before that, she was a Lise Meitner postdoctoral researcher in the Visual Computing and AI Department at Max Planck Institute for Informatics. She obtained her Ph.D. degree from the University of Hong Kong in 2019. Her research interests are Neural Scene Representations, Neural Rendering, Human Performance Modeling and Capture, and 3D Reconstruction.

Adam Kortylewski is a research group leader at the University of Freiburg and the Max Planck Institute for Informatics where he leads the Generative Vision and Robust Learning lab. Before that he was a postdoc at Johns Hopkins University with Alan Yuille for three years. He obtained his PhD from the University of Basel with Thomas Vetter. His research focuses understanding the principles that enable artificial intelligence systems to reliably perceive our world through images. Adam was awarded the prestigious Emmy Noether Grant (2022) of the German Science Foundation for exceptionally qualified early career researchers.

Christian Theobalt is a Professor of Computer Science and the director of the department “Visual Computing and Artificial Intelligence” at the Max Planck Institute for Informatics, Germany. He is also a professor at Saarland University. His research lies on the boundary between Computer Vision and Computer Graphics. Christian received several awards, for instance the Otto Hahn Medal of the Max Planck Society (2007), the EUROGRAPHICS Young Researcher Award (2009), the German Pattern Recognition Award (2012), an ERC Starting Grant (2013), an ERC Consolidator Grant (2017), and the Eurographics Outstanding Technical Contributions Award (2020). In 2015, he was elected one of Germany’s top 40 innovators under 40 by the magazine Capital.

Eric Xing (Fellow, IEEE) received the Ph.D. degree in computer science from the University of California at Berkeley, Berkeley, CA, USA, in 2004. He is currently a Professor of machine learning with the School of Computer Science, Carnegie Mellon University, Pittsburgh, PA, USA. His principal research interests lie in the development of machine learning and statistical methodology, especially for solving problems involving automated learning, reasoning, and decision-making in high-dimensional, multimodal, and dynamic possible worlds in social and biological systems. Dr. Xing is a member of the DARPA Information Science and Technology (ISAT) Advisory Group and the Program Chair of the International Conference on Machine Learning (ICML) 2014. He is also an Associate Editor of The Annals of Applied Statistics (AOAS), the Journal of American Statistical Association (JASA), the IEEE Transactions on Pattern Analysis and Machine Intelligence (T-PAMI), and PLOS Computational Biology and an Action Editor of the Machine Learning Journal (MLJ) and the Journal of Machine Learning Research (JMLR).